High strain rate properties of metals and alloys

R. W. Armstrong*[1] and S. M. Walley[2]

The high strain rate dependence of the flow stress of metals and alloys is described from a dislocation mechanics viewpoint over a range beginning from conventional tension/compression testing through split Hopkinson pressure bar (SHPB) measurements to Charpy pendulum and Taylor solid cylinder impact tests and shock loading or isentropic compression experiment (ICE) results. Single crystal and polycrystal measurements are referenced in relation to influences of the crystal lattice structures and nanopolycrystal material behaviours. For body centred cubic (bcc) metals, the strain rate sensitivity (SRS) is in the yield stress dependence as compared with the face centred cubic (fcc) case of being in the strain hardening property. An important consequence is that an opposite ductility influence occurs for the tensile maximum load point strain that decreases with strain rate for the bcc case and increases with strain rate for the fcc case. Different hexagonal close packed (hcp) metals are shown to follow either the bcc or fcc case. A higher SRS for certain fcc and hcp nanopolycrystals is explained by extrapolation from conventional grain sizes of an inverse square root of grain size dependence of the reciprocal activation volume determined on a thermal activation strain rate analysis (TASRA) basis. At the highest strain rates, additional deformation features enter, such as deformation twinning, adiabatic shear banding and very importantly, for shock induced plasticity, transition from plastic flow that is controlled by the mobility of the resident dislocation density to plasticity that is controlled by dislocation or twin generations at the shock front. The shock description is compared with the very different high rate shockless ICE type loading that occurs over nanoseconds and leads to higher compressive strength levels because of dislocation drag resistance coming into play for the originally resident mobile dislocation density. Among the high strain rate property, concerns are the evaluation of ductile to brittle transition behaviours for bcc and related metals and also, projectile/target performances in ballistic impact tests, including punching. Very complete metallographic and electron microscope observations have been reported in a number of the high rate deformation investigations.

Keywords: Dislocation mechanics, High strain rates, Thermal activation, Single crystals, Nanopolycrystals, Shock induced plasticity

Introduction

Almost from the earliest time of stress–strain measurements being reported for the conventional strain rate (and temperature) dependences of the deformation and fracturing behaviours of metals and alloys, there were concerns about the connection of such measurements with the higher strain rate properties of the same materials. A special early concern was to relate an apparent mismatch between the essentially static tensile or compressive test results, for which an approximately linear dependence of flow stress on the logarithm of strain rate occurred, and those higher flow stresses derived from generally more complicated dynamic material test results. The dilemma gained importance during the late 19th century when specification of both representative load–displacement and stress–strain behaviours were being first reported for various metals and their alloys.

Selected historical references

That the properties of materials under impact differed from those determined under static or 'dead' loading conditions was reported in early researches done by J. Hopkinson.[1–3] The work was followed up later in one report by his son, B. Hopkinson,[4] who also reported further later on the shapes of pulses produced by bullet impact and on the pulse shapes produced by explosive

[1]University of Maryland, College Park, MD 20742, USA
[2]University of Cambridge, Cambridge CB3 0HE, UK

*Corresponding author, email rona@eng.umd.edu

Published by Maney for the Institute and ASM International
DOI 10.1179/174328008X277795

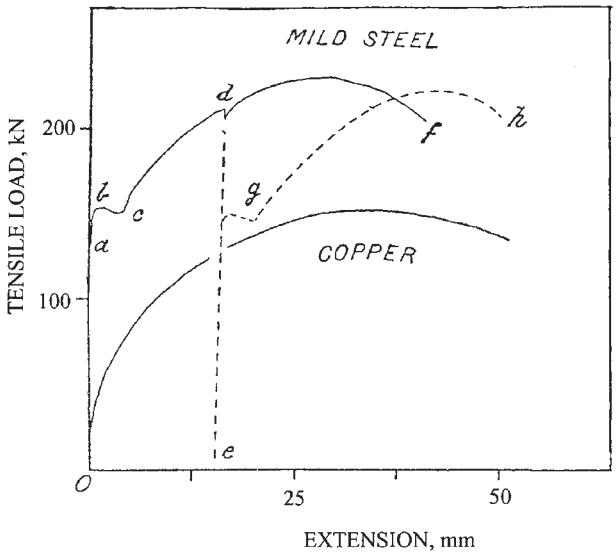

1 Representative tensile load–extension curves for copper and steel, adapted from results reported by Unwin[11,12]

detonators.[5] The latter work has modern relevance to be described in the present review, for example, to obtaining pressure measurements such as reported very recently on an insensitive munitions basis for bullet impact and shaped charge ordnance concerns by Niles *et al.*[6] And later, Charpy,[7] reported on the development of the impact pendulum test involving a notched specimen. Toth *et al.*[8] have produced a historical description of the impact pendulum test as part of a 2001 centennial meeting to honour Charpy's first published work on the topic. Particular attention is given in the report to the establishment over time of engineering standards that have led to the current employment of instrumented Charpy impact tests. Metal working methods, including forging, were also to have influence on the consideration of changed material behaviours under dynamic loading conditions. The description by Tresca[9] of 'adiabatic heat lines' in forging is credited by Johnson[10] to have provided the earliest evidence of shear banding behaviour.

Early results on the engineering documentation of different yielding and plastic deformation behaviours observed for copper and steel materials were reported on a load–extension basis by Unwin[11] and are shown on a comparative graph in Fig. 1, as adapted from the original results by Armstrong and Zerilli.[12] A point to be made later in the current review is that an increase in strain rate moves the maximum load point (instability) of steel to smaller deformation whereas the reverse effect occurs for copper; and, these characteristics are representative of metals with either body centred cubic (bcc) or face centred cubic (fcc) lattice structures respectively. With respect to the typical yield point consideration initially associated only with carbon in iron and with related bcc metals, however, McReynolds[13] has reported the occurrence also of yield point and serrated yielding behaviours even in sensitive tensile tests of pure (99·996%) aluminium and aluminium alloy materials investigated with respect to the loading rate. It is interesting to note that at the same time of Unwin's report, Ewing[14] made the important distinction between small strain measurements being made either in a single material test specimen or within a larger engineering structure; the point here relating to the observation by Orowan[15] that information taught in early 'strength of materials' courses, the origin of which has been credited to Mohr of 'Mohr circle' fame, actually was mechanics based 'strength of structures' knowledge taught as though the strength of the material was already known. Also, Orowan returned in the same report to the issue of the notch brittleness of steel materials, as measured in the Charpy V notch test, and directed further attention then to the importance of X-ray diffraction in establishing an understanding of structure/property relations, as followed from the first Nobel Prize in Physics being awarded to Roentgen for the discovery of X-rays, and now via X-ray diffraction being very much involved in probing crystallographic aspects of shock induced material structures, as reported, for example, by Wark *et al.*[16] Last, relating to the maximum load points observed for copper and steel in Fig. 1 is the consideration of their being points of tensile instability and specified by the so called Considère[17] condition

$$\sigma = \mathrm{d}\sigma/\mathrm{d}\varepsilon \tag{1}$$

where σ is the true stress, ε is the true strain and $\mathrm{d}\sigma/\mathrm{d}\varepsilon$ is the true strain hardening. As will be seen, current interest continues in the employment of equation (1) as applied to metal and alloy behaviours extended even to extremely suddenly applied high pressure conditions and thus, involving material behaviours at the highest strain rates achievable, for example, in shock testing or in isentropic compression experiments (ICE).

Current purview

Here, the high strain rate properties of metals and alloys are reviewed with particular emphasis on the development of dislocation mechanics based constitutive equations that are mainly employed in material dynamics calculations. The material behaviours are described over a range of strain rates beginning from conventional tensile or compressive stress–strain measurements through solid cylinder (Taylor) impact and split Hopkinson pressure bar (SHPB) measurements to shock loading and most recently, ICE results. Lattice structure and single crystal to polycrystal to nanopolycrystal measurements and their constitutive equation descriptions are covered. Because the strain rate sensitivity (SRS) is in the yield stress of bcc metals as compared to being in the strain hardening of fcc metals, the maximum load point strain shown in Fig. 1 moves to smaller strains for bcc metals and larger strain for fcc metals. Some hexagonal close packed (hcp) metals behave similarly to bcc ones and others follow the fcc case, that for purer compositions exhibit a grain size dependence of the SRS that is greatly magnified at nanopolycrystal grain sizes. At the highest strain rates, additional deformation features come into play of deformation twinning, adiabatic shear banding and very importantly for shock induced plasticity, a transition occurs from plastic flow being controlled by mobility of the resident dislocation density to plasticity being controlled by defect generation at the shock front. Significant concerns of high strain rate loading are the onset of a ductile–brittle transition in behaviour for bcc metals and related materials as well as projectile/target performances in ballistic impact tests, including 'punching'.

Topics not to be covered in the present review, despite their own importance, are:

(i) low stress dependent creep behaviours at low strain rates and related superplasticity behaviours at higher rates
(ii) metal forming conditions/applications normally achieved at intermediate strain rates
(iii) delayed yielding phenomena, for example, as described by Suh and Lee,[18] for polycrystal grain size influences even for delayed flow associated ultimately with dynamic Hopkinson type deformation velocities
(iv) the fundamental mechanisms determining dislocation drag coefficients (*see*, for example, the article by Mason[19])
(v) at the highest imaginable strain rates, Lagrangian dependent dislocation velocity influences; *see* Ref. 20 for retention here of the static form

$$F = \tau b \tag{2}$$

for the dynamic dislocation force per unit length F in terms of the shear stress τ and the dislocation Burgers vector b as compared with an alternate description offered by Hirth and Lothe.[21] And, among other texts and reviews on the general subject are, for example, those by Rinehart and Pearson,[22] Meyers[23] and Edwards.[24]

Early measurement/constitutive equation connections

In the first quarter of the twentieth century, the strain rate dependences of engineering material properties were being measured in standard tensile/compressive tests, also, as part of investigations into associated temperature and polycrystal grain size dependences, for example as described by Jeffries.[25] Also, during this early period, the strain rate dependences of individual crystals were being investigated as they became available for research studies, either by cutting individual crystals from large grained polycrystalline specimens or by direct production of individual crystals. An early twentieth century result on static and dynamic testing of individual iron crystals was reported by Osmond and Frémont[26] including their mention of dynamic deformation and cleavage results for a few individual iron crystal beams impacted in flexural tests.

Measurements and model analysis were presented for the strain rate (and temperature) dependence of zinc and iron single crystal viscoplastic behaviours in the PhD thesis done at Goettingen by Brezina,[27] who referenced von Karman and acknowledged encouragement received from Prandtl, in proposing the plastic strain rate relationship for the complete stress–strain dependence

$$\frac{\mathrm{d}\varepsilon_\mathrm{p}}{\mathrm{d}t} = a\exp(\beta\sigma - \chi\varepsilon) \tag{3}$$

where a, β and χ were taken as experimental constants; note the dependence of σ on $\log(\mathrm{d}\varepsilon_\mathrm{p}/\mathrm{d}t)$ at constant ε. Other thermally activated plastic flow descriptions were soon reported by Becker[28–30] and Eyring.[31,32] Eyring developed thermally activated, chemical reaction type, strain rate equations similar to those proposed by Prandtl and Becker and as will be seen, to dislocation mechanics based constitutive equations proposed by

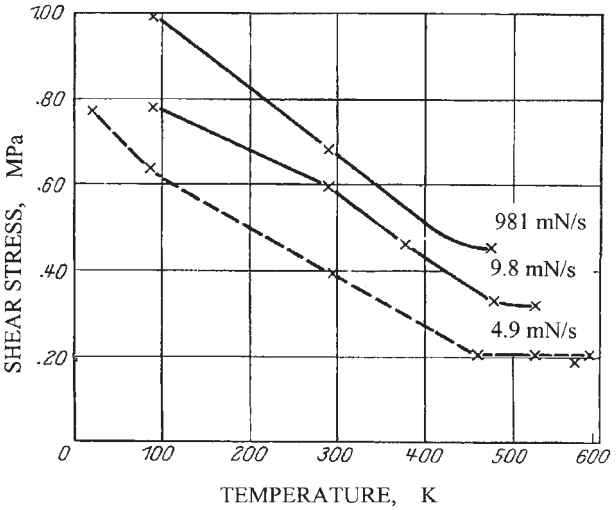

2 Cadmium single crystal resolved shear stresses *v.* absolute temperature for different 'speeds of stressing' in mN s^{-1}, as adapted from pioneering results reported by Schmid and Boas[38]

Orowan, Taylor and Polanyi. Among others following on in the same vein as Eyring were Kauzmann,[33] for a thermal activation–strain rate analysis (TASRA) expression obtained in terms of rather unspecified 'flow units' and also, Seitz and Read[34] in a number of articles.

Advent of dislocation mechanics

The thus established viscoplastic character of post-yield plastic deformation was the basis for two of the researchers, Orowan[35] and Polanyi,[36] arriving at the 1934 'invention' of crystal dislocations, as compared with the same year alternative level of strength consideration leading Taylor[37] to the same model consideration. The model developments were in line with a multitude of experimental test results being reported on single crystal plasticity properties and their crystallographic aspects as reported, for example, in the crystal plasticity book of Schmid and Boas;[38] *see* Fig. 2 for the reported temperature dependence of the critical resolved shear stress of cadmium crystals measured at different 'speeds of stressing'. The original dislocation mechanics descriptions were followed by a seminal article by Orowan[39] who provided the fundamental dislocation determined strain rate description in either one of two forms

$$\frac{\mathrm{d}\varepsilon}{\mathrm{d}t} = \frac{1}{m}\rho b v \tag{4}$$

or

$$\mathrm{d}\varepsilon/\mathrm{d}t = (1/m)(\mathrm{d}\rho/\mathrm{d}t)b\Delta x_\mathrm{d} \tag{5}$$

where m is an orientation factor for resolution of the strain tensor, ρ is the dislocation density, expressed in line length per unit volume, v is the average dislocation velocity, $\mathrm{d}\rho/\mathrm{d}t$ is the rate of dislocation generation and Δx_d is the average distance moved by the dislocations. Equation (4) has evolved as the standard relation to be employed at low and intermediate strain rates. As will be seen in the present review, equation (5) is newly proposed for application to plasticity control by dislocation, or deformation twin, generation at a propagating shock front. It is notable that it was an interest in

viscoplasticity, plus the crystal properties research interest of brother, W. G. Burgers, that played an important part in attracting the attention of the fluid dynamicist, J. M. Burgers,[40] to dislocation properties and the eventual eponymous assignment of 'Burgers vector' b to the dislocation translation vector.

Dynamic plasticity

Zener and Hollomon[41] reported both a constitutive equation for the coupled strain rate/temperature dependences for iron and steel materials in the relationship

$$\sigma/\sigma_0 \sim \left\{\left[(\mathrm{d}\varepsilon/\mathrm{d}t)/(\mathrm{d}\varepsilon/\mathrm{d}t)_0\right]\exp(Q/RT)\right\}^r \tag{6}$$

and provided a stress–strain and metallographic description of adiabatic shear banding in several steel materials 'caused by an increase in strain rate', particularly for low temperature tests. In equation (6), σ_0 and $(\mathrm{d}\varepsilon/\mathrm{d}t)_0$ are reference flow stress and strain rates respectively, Q is an activation energy, R is the gas constant, T is temperature and r is an experimental constant. Near to the same time, Taylor[42] proposed the designation of 'dynamic yield strength' for the flow stress of materials subjected to rapid deformation. And in the same period, Barrett and Haller, Jr,[43] reported for tests on polycrystalline magnesium an increased occurrence of deformation twinning that was produced by imposing an increased 'speed of deformation'.

A new solid cylinder impact test was developed at the time by Taylor and colleagues,[44–46] consistent with determination of an average 'dynamic yield strength' of a material from the cylinder change in length after impact onto a rigid target. Taylor[44] obtained the relation

$$\sigma = \left(\rho_c v_c^2/2\right)(L-X)/(L-L_1)\ln(L/X) \tag{7}$$

for which ρ_c is the material density, v_c is the impact velocity, L is the original cylinder length, X is the length of the undeformed part of the cylinder and L_1 is the final total length of the cylinder. Whiffin[45] reported on the results obtained with solid cylinders of various metals and alloys. In turn, Carrington and Gayler[46] reported on metallurgical aspects of the test results. Figure 3 shows a longitudinally sectioned specimen after impact and for which post-impact hardness measurements are identified as a function of position on the sectioned surface. A dashed boundary is shown to demarcate the harder impacted region that was associated also with the presence of (deformation twins described then as) impact initiated Neumann bands. The pioneering work of Taylor and colleagues was followed by a further supporting analysis provided by Hawkyard *et al.*.[47] Both the Taylor *et al.* and Hawkyard *et al.* investigations, and many others, have been recently reviewed in detail by Chapman *et al.*.[48]

The strain rates operative in the Taylor solid cylinder impact test are known today to span those measured with the Hopkinson pressure bar. During the period of development of the Taylor test, Davies[49] provided a detailed analysis of the SHPB testing technique and Kolsky[50] provided the equations

$$\sigma = E_{\mathrm{bar}}(A_0/A)\int (\mathrm{d}\varepsilon/\mathrm{d}t)_T \mathrm{d}t \tag{8}$$

and

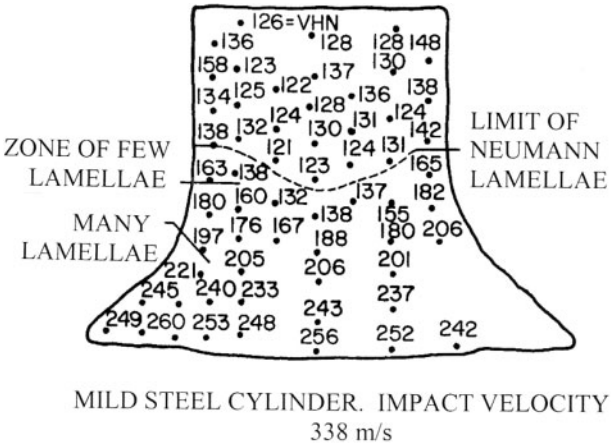

3 Longitudinally sectioned, original Taylor impact test specimen of mild steel, with position dependent Vickers hardness numbers (VHN) and demarcated (dashed) boundary defining lower impact region where Neumann lamellae (now known as deformation twins) had been formed during impact, as adapted from results reported by Carrington and Gayler;[46] VHN in kg mm^{-2} is multiplied by 9·81 to obtain hardness pressure in MPa

$$\mathrm{d}\varepsilon/\mathrm{d}t = -(2c_0/L)\int (\mathrm{d}\varepsilon/\mathrm{d}t)_R \mathrm{d}t \tag{9}$$

in which E_{bar} is the Young's elastic modulus of the bar, A_0 and A are the initial and current cross-sectional areas of the specimen, with the subscript T for the transmitted stress wave, c_0 is the elastic wave speed, L is specimen length and the subscript R applies for the reflected wave. Later interest of Kolsky in the fracturing of glass by free surface reflection of the compressive wave at the bar end as a tensile wave was extended to basal (0001) cleavages of [0001] rod axis oriented zinc crystals.[51] B. Hopkinson[4] had commented on the compressive to tensile wave conversion caused by reflection at the free surface end of the bar. The pressure bar technique also attracted the attention of von Karman and Duwez[52] who developed the following relations for their own deformation measurements produced by a 'plastic wave' causing the impacted extension of wires of copper or iron materials

$$v_i = \int [(\mathrm{d}\sigma/\mathrm{d}\varepsilon)/\rho_c]^{1/2}\mathrm{d}\varepsilon \tag{10}$$

and

$$v_p = [(\mathrm{d}\sigma/\mathrm{d}\varepsilon)/\rho_c]^{1/2} \tag{11}$$

The preceding experimental results and derived relationships were shown by Armstrong and Zerilli[53] to be in reasonable agreement with predictions from a dislocation mechanics based description of the behaviours, as shown in Figs. 4 and 5, and which constitutive relations are to be described below.

Kolsky's researches on the SHPB were followed by descriptions of tensile bar set-ups developed by Harding *et al.*[54] and by Nicholas.[55] A torsion bar system was developed by Hartley *et al.*.[56] Review articles on the SHPB were provided by Follansbee[57] and by Gray, III.[58] Application of the SHPB method to fracture toughness testing was developed by Klepaczko.[59] The current status of researches based on SHPB testing has

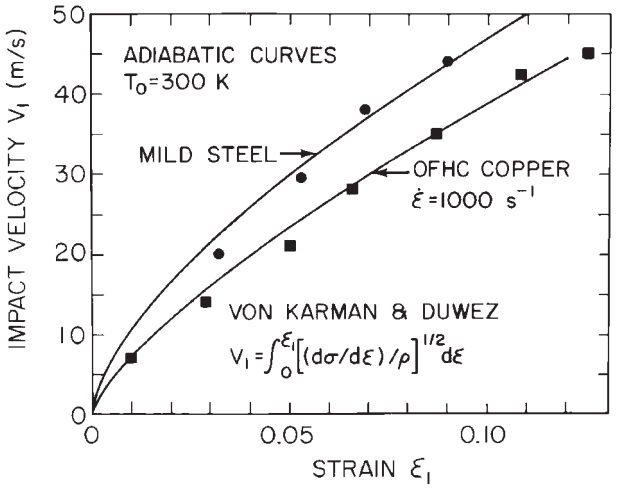

4 Predicted relationship of tensile impact velocity and consequent strain measurements for copper and steel materials investigated by von Karman and Duwez,[52] as evaluated here in terms of separate fcc and bcc dislocation mechanics based equations reported by Armstrong and Zerilli[53] for other experimental measurements

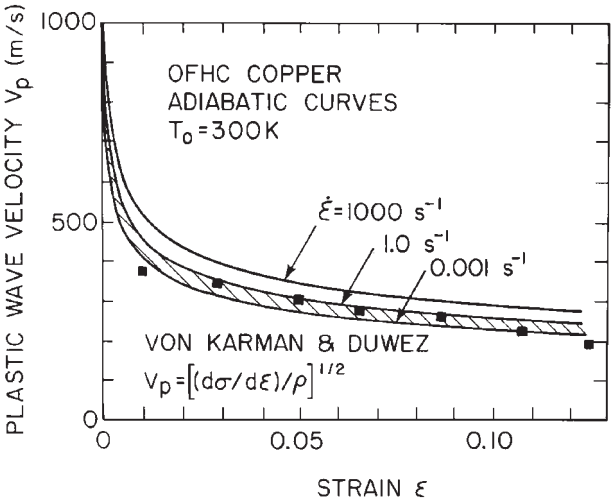

5 Predicted relationship of 'plastic wave' velocity and strain measurements for copper, reported by von Karman and Duwez,[52] as evaluated in terms of fcc dislocation mechanics based equation applied by Armstrong and Zerilli[53] to other experimental measurements

been reviewed most recently by Field *et al.*,[60] included in their 'Table 1'. Developments in high strain rate testing', reference to the first high strain rate mechanical testing machine having been built by Dunn.[61] And Fig. 6, after Kolsky,[50] was taken from the review. Experimental issues of specimen size, time for stress equilibrium, temperature gradient, wave dispersion and influence of radial inertia were described by Field *et al.* Later research references are to Vecchio and Jiang[62] for advantageous pulse shaping in the SHPB test and to Jiang and Vecchio[63] for SHPB designed four point fracture test results. A further note of interest on the SHPB concerns the development at the University of Cambridge of a miniature diameter, direct impact, Hopkinson bar for inertia reduction at very high strain rates.[64–66] Miniature SHPB systems have recently been developed for obtaining data on nanocrystalline and amorphous materials at the upper limits of one-dimensional stress testing (10^5 s^{-1}).[67–69]

Dislocation dynamics

Seminal descriptions of dislocation dynamics in plasticity are provided: first, in an update of single crystal deformation properties in terms of the TASRA given in a summary article by Seeger;[70] and second, covering more broadly the status of dislocation dynamics until 1967, in the symposium proceedings co-edited by Rosenfield *et al.*[71] Particular articles in Rosenfield *et al.* of special relevance to the current purpose are the following: Li, 'Kinetics and dynamics in dislocation plasticity', 87–116; Taylor, 'Stress wave profiles in several metals', 573–589; Butcher and Munson, 'The application of dislocation dynamics to impact-induced deformation under uniaxial strain', 591–607; and Campbell, Cooper and Fischhof, 'The dynamics of non-uniform plastic flow in low carbon steel', 723–746.

Lattice and microstructural influences

In a series of articles, Zerilli and Armstrong[72–78] developed a set of dislocation mechanics based constitutive relations for employment in computational codes, such as elastic–plastic impact calculation (EPIC), applied to modelling of material dynamics. The purpose was to base such relations on mechanistic dislocation behaviours while minimising the number of experimental parameters needed to adequately describe the material responses. Critical to the simplification of the equations was employment of an inverse dependence on the thermal component of stress of the dislocation activation volume V^* (Ref. 79)

$$V^* = A^* b = k_B T[\partial \ln(d\varepsilon/dt)/\partial \tau^*]_T = W_0/\tau^* \qquad (12)$$

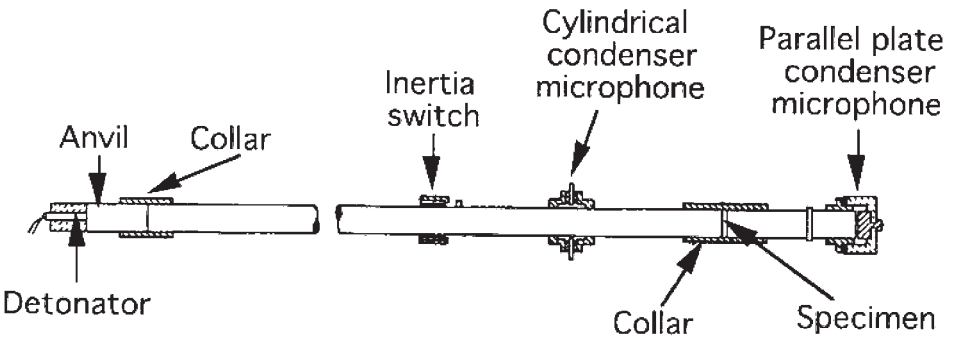

6 Schematic description of SHPB apparatus reported by Kolsky,[50] as described in review by Field *et al.*[60]

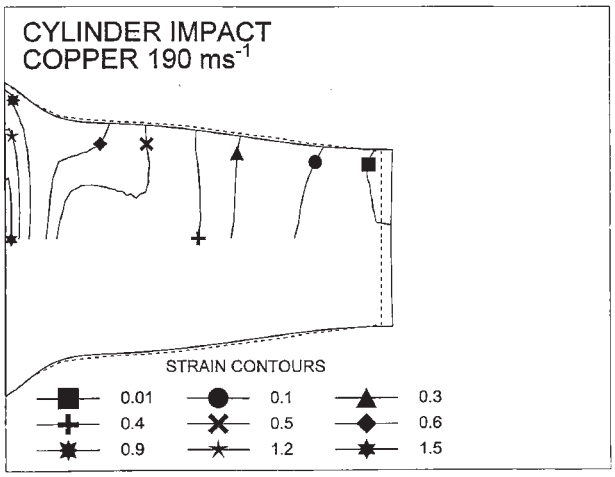

7 Longitudinally sectioned solid cylinder Taylor impact test result for OFHC copper measurements of Johnson and Cook,[103,104] as matched with shape prediction obtained from Zerilli–Armstrong constitutive equation description[72] and including position sensitive isostrain contours within predicted shape

in which A^* is the TASRA based activation area, k_B ($=1{\cdot}38\times10^{-23}$ J K^{-1}) is Boltzmann's constant, τ^* is the thermal component of stress associated with the change in strain rate and the experimental constant $W_0=3{\cdot}1\times10^{-20}$ J. The reciprocal value of V^* is employed as one measure of the SRS of a material (*see* the section on 'Current purview'). Zerilli[80] has provided a summary description of the so called Z–A relations, employing equation (12) and other dislocation model characteristics, in a combined form for the flow stress σ as

$$\sigma=\sigma_a+B\exp(-\beta T)+B_0\{\varepsilon_r[1-\exp(-\varepsilon/\varepsilon_r)]\}^{1/2}\exp(-\alpha T) \quad (13)$$

$$\sigma_a=\sigma_G+k_\varepsilon l^{-1/2} \quad (14)$$

$$(\beta,\alpha)=(\beta_0,\alpha_0)-(\beta_1,\alpha_1)\ln(\mathrm{d}\varepsilon/\mathrm{d}t) \quad (15)$$

where σ_G is an athermal stress,[70] dependent on the material shear modulus G, k_ε is the microstructural stress intensity for transmission of plastic flow at grain boundaries,[81] l is the polycrystal grain diameter, ε_r is a reference strain for the onset of dynamic recovery at larger strains,[78] and B, β, B_0, α, β_0, α_0, β_1 and α_1 are experimental constants.

The temperature and strain rate dependences for fcc metals and alloys, except for k_ε, are largely in the material strain hardening behaviour that is controlled by the TASRA based overcoming of dislocation intersections. Klepaczko[82] has provided a review of the fcc case. Thus, equations (13) and (15) are relatively simplified because of

$$B=\beta=\beta_0=0 \quad (16)$$

Also, for the normal stress–strain case of $\varepsilon/\varepsilon_r<1{\cdot}0$, the strain hardening term in equation (13) approximates to a simplified parabolic strain dependence, that is so called Taylor strain hardening.[78] With such parabolic strain hardening and with experimental constants determined from other experimental results, the Taylor cylinder impact results shown in Fig. 7 were computed for copper.[72] More recently, Eakins and Thadhani[83] have optically tracked the transient shape changes developed in Taylor tests of oxygen free electronic (OFE) copper material and made favourable comparisons with predicted results from the Z–A and other constitutive equation descriptions to be further described in the present article. In an accompanying investigation, these same authors[84] reported the determination of isostrain plastic wave velocities and corresponding average dynamic flow stress estimations.

For the bcc case, the temperature and strain rate dependence is in the yield stress property and the material strain hardening is essentially athermal and thus, in equation (13)

$$\alpha=\alpha_0=0 \quad (17)$$

Figure 8 shows the fit of equation (13), subject to the equation (17) condition and with an athermal strain hardening exponent of 0·44, to pioneering experimental results reported by Hoge and Mukherjee[85] for the tensile stress–strain behaviour of tantalum material that was tested over a wide range of temperatures and strain rates. Also, the tensile uniform strain was computed according to the Considère condition of equation (1) and its locus is shown in the figures in comparison with the reported measurements. Figure 8*b* provides confirmation of the maximum load point moving to smaller strain for the bcc case. Measurements of the uniform strain reduction with increase in strain rate are compared with computed results in Fig. 9; in the figure legend, $K=B_0$ in equation (13). Also, for tantalum material, Chen *et al.*[86] had reported the stress–strain behaviour at sufficient strains that Zerilli[80] could show the influence of the strain dependent dynamic recovery correction in equation (13) involving ε_r (*see* Fig. 10).

Hexagonal close packed metals and alloys follow either the bcc or fcc cases. Thus, titanium and Ti–6Al–4V alloy have been shown to follow the bcc case, with added complications of deformation twinning.[77,87] Magnesium, zinc and cadmium, however, follow the fcc case, with significant grain size dependences in agreement with equation (14) and with important temperature and strain rate dependences also in k_ε. Armstrong[79] showed that both the 'friction stress' intercept $\sigma_0=m(\tau_G+\tau^*)$ and microstructural stress intensity k_ε could show separate TASRA based dependences through the thermal component of shear stress τ^* and τ_C, the local shear stress for plastic flow in the grain boundary regions, as contained in the relations

$$\sigma=m[(\tau_G+\tau^*)]+k_\varepsilon l^{-1/2} \quad (18)$$

and

$$k_\varepsilon=m(\pi m_S G b\tau_c/\alpha)^{1/2} \quad (19)$$

in which m_S is a Sachs orientation factor and an average dislocation character is expressed in the factor $\alpha=2(1-\nu)/(2-\nu)=\sim0{\cdot}8$, with ν being Poisson's ratio. For magnesium, the temperature dependence of the friction stress was matched with that of the critical resolved shear stress for basal, (0001)<11–20>, slip while the temperature dependence of k_ε^2 was matched with that of more difficult prism, {10–10}<11–20>, slip, as adapted from Armstrong[88] in Fig. 11. Similar results have been reported for zinc[89] and cadmium,[90] the grain boundary

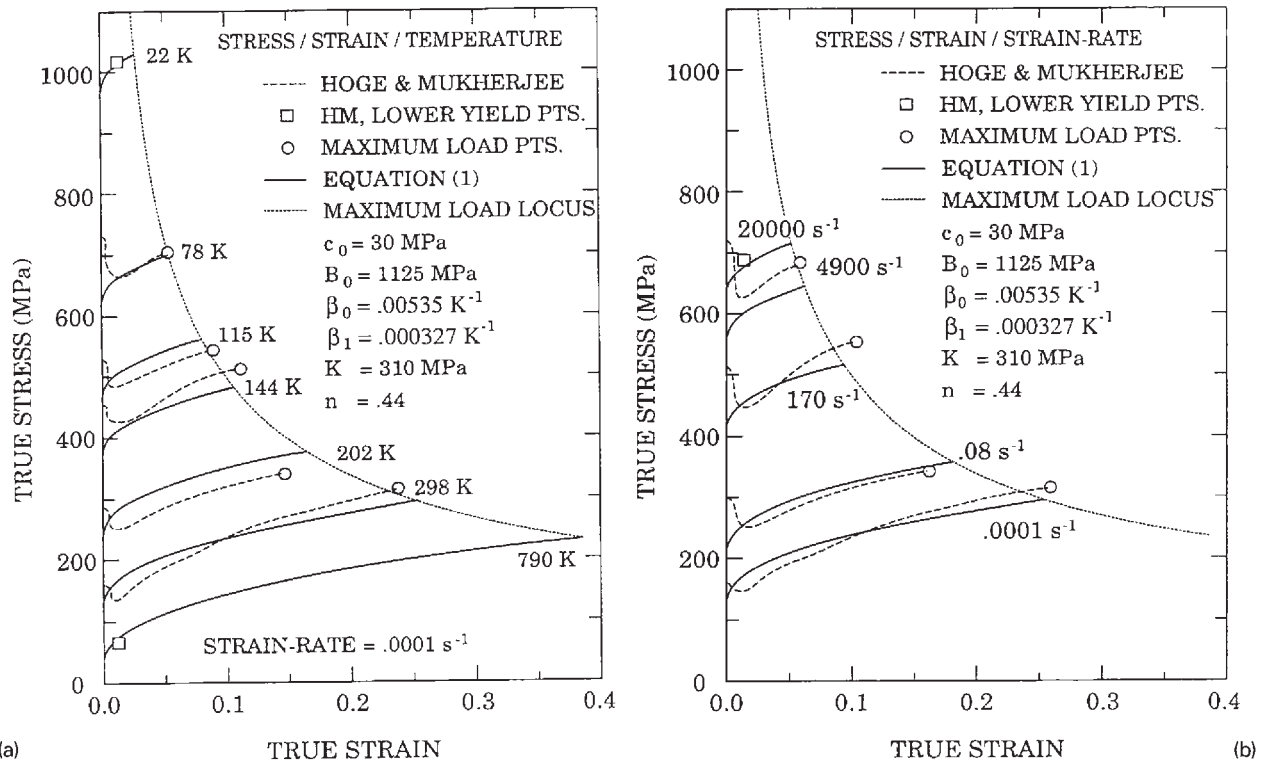

8 Comparison of measured[85] and computed[75] tensile stress–strain curves, also including locus for maximum load stress, for polycrystalline tantalum: *a* at fixed strain rate for different temperatures in range 22 to 790 K and *b* for strain rates in the range 10^{-4} to $2\times10^{+4}$ s^{-1} at 298 K; in figure legends, equation (1) is equation (13) in text subject to condition of equation (17) and $c_0=\sigma_a$, $B_0=B$ and strain hardening term $K\varepsilon^n$ replaces last term of equation (13)

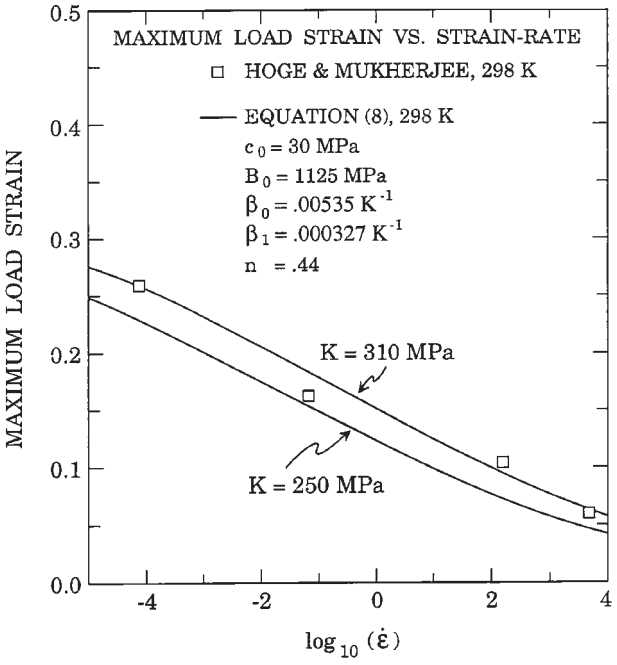

9 Comparison at 298 K of measured[85] and computed[75] tensile maximum load strains for polycrystalline tantalum material as function of strain rate and employing two strain hardening coefficients *K*; *see* caption of Fig. 8 for definition of symbols applicable to equation (1) in that figure legend, as derived from substitution of Z–A bcc equation into reference equation (1) subject to maximum load condition, that is equation (1) in present text

deformation behaviours of which have been shown to be controlled by pyramidal, {10–11}<11–21>, slip. For fcc copper and nickel, Rodriguez[91] has reviewed the evidence that dislocation intersections within the grains control the friction stress whereas cross-slip controls deformation in the grain boundary regions. Figure 12 shows the match of experimental measurements reported for copper by Armstrong[91,178] of the temperature and strain rate dependencies of k_ε^2 and the cross-slip stress τ_{III}. Zhu *et al.*[92] have provided model calculations of slip transfer reactions at nanotwin boundaries in copper. The high ductility of such material is attributed to the accompanying twin boundary hardening

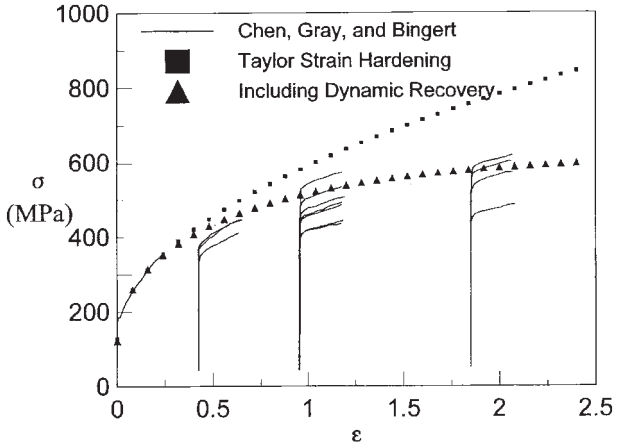

10 Computed full stress–strain curves,[80] at strain rate of 10^{-3} s^{-1} at 298 K and to large strains, for tantalum in comparison with separate series of experimental stress–strain measurements made after different extents of straining by Chen *et al.*[86]

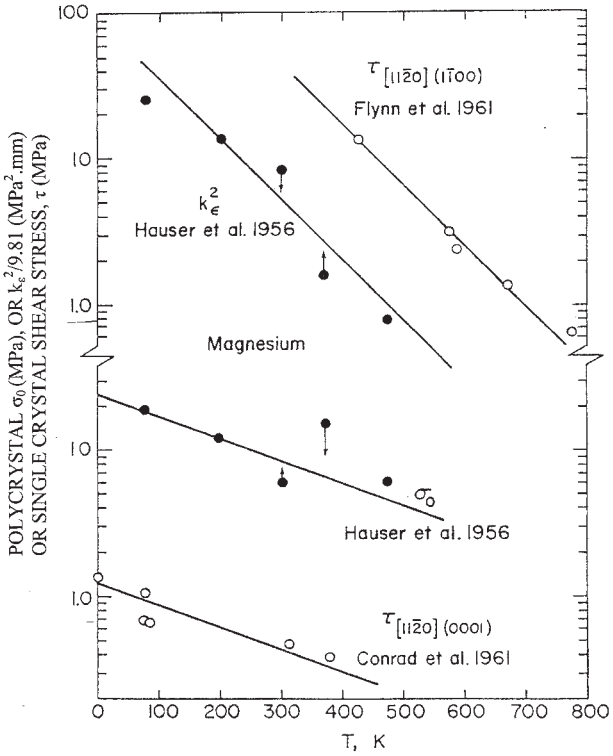

11 Predicted match of temperature dependences for polycrystal stress–grain size σ_0 and k_ϵ^2 parameters with corresponding measurements of single crystal basal and prism slip system stresses respectively, as assessed by Armstrong[88] from measurements reported on polycrystalline magnesium

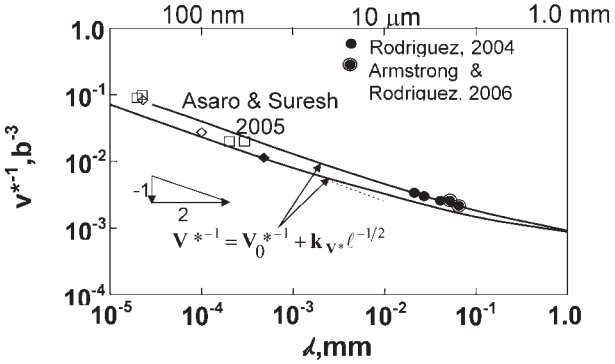

13 TASRA based prediction of grain size dependence of reciprocal activation volume V^{*-1} at conventional grain sizes and extrapolated to show agreement with measurements assembled for nanocrystalline copper and nickel materials:[95] b is dislocation Burgers vector and grain diameter $d=l$

associated with the slip transfers and the gradual loss of the boundary coherencies. In other recent cross-slip model simulations, Wang *et al.*[93,94] have focused attention on the increasing importance of cross-slip in their simulations of high rate deformations, especially, in connection with model predictions of enhanced dislocation generations.

The model consideration of a grain size dependent TASRA based influence on k_ε leads then to a grain size dependent value of the reciprocal polycrystal activation volume V^{*-1} of the form

$$V^{*-1} = V_0^{*-1} + \left(k_\varepsilon / 2m\tau_C V_C^*\right) l^{-1/2} \tag{20}$$

in which the subscripts 0 and C apply for within the grains and at the grain boundaries respectively, and at low strains, the product $\tau_C V_C^*$ is reasonably constant at $3{\cdot}1 \times 10^{-20}$ J, as mentioned above for equation (12), so that a reciprocal grain size dependence of the same form as equation (14) obtains. Armstrong and Rodriguez[95] have applied equation (20) to interpretation of a strong grain size dependence of nanopolycrystal SRS measurements for copper and nickel previously compiled by Asaro and Suresh,[96] as shown in the log/log graph of Fig. 13; *see* also the review on nanopolycrystal materials by Meyers *et al.*.[97] Recently, Conrad[98] has developed a somewhat different TASRA description for the effect of grain size on the 'plastic deformation kinetics' in the

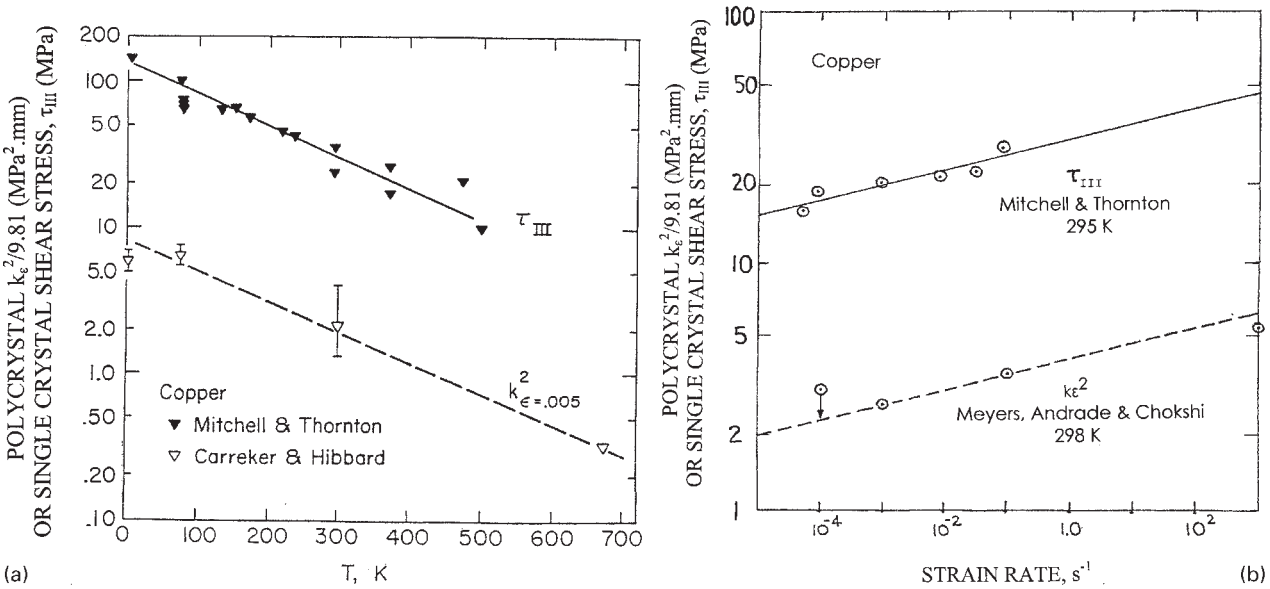

12 Predicted match of *a* temperature and *b* strain rate dependent copper polycrystal k_ϵ^2 and single crystal resolved shear stresses for cross-slip τ_{III} measurements[91,178] respectively

20–500 nm grain size regime. It should be mentioned, however, in the present connection that the TASRA dependence in k_ε only applies for relatively small grain size dependences, as will be discussed below in connection with grain size aspects of deformation twinning, fracture, and concerning the role of dislocation pile-ups in providing a fundamental explanation of adiabatic shear banding.

Relation to other constitutive analyses

Gilman[99] produced an early dislocation dynamics relation building onto the Orowan[39] description of equations (4) and (5) as

$$\mathrm{d}\varepsilon_\mathrm{p}/\mathrm{d}t = mbv^*\left(N_0 + M^*\varepsilon_\mathrm{p}\right)\exp\left[-\left(D + H\varepsilon_\mathrm{p}\right)/\tau\right] \quad (21)$$

where v^* is the upper limiting dislocation velocity, N_0 is the initial dislocation density, M^* is the strain coefficient for dislocation density build-up, and D and H are material constants implicitly dependent on the temperature. A complementary description of constitutive relations to those in equations (13)–(15) and differentiating between fcc and bcc metal behaviours on a dislocation density basis has been reported by Voyiadjis and Abed.[100,101] These authors have proposed modification of equations (13)–(15) leading to new relations more generally applicable above 300 K and at more elevated temperatures.[102] Here, attention is directed to the so called Z–A equations (13)–(15) having been developed on a dislocation mechanics basis for use in hydrocode calculations of material dynamics behaviours in the same way as had been done for the very effective numerically based Johnson–Cook[103,104] equations employed in the EPIC hydrocode as

$$\sigma = (a + B'\varepsilon^\mathrm{n})[1 + C\log(\mathrm{d}\varepsilon/\mathrm{d}t)](1 - T^{*\mathrm{m}}) \quad (22)$$

in which a, B', n, C and m are experimental constants and $T^* = (T_\mathrm{m} - T)/(T_\mathrm{m} - T_\mathrm{r})$ with T_m being the melting temperature and T_r being room temperature (*see* Ref. 105 for a recent account of determining the constants). Normally, for comparison with any TASRA based relation, the alternative of a power law relation is employed, for example as described by Nemat-Nasser *et al.*[106] in terms of shear stress τ and shear strain γ as

$$\tau = \tau_0[1 + (\gamma/\gamma_0)]^\mathrm{N}[(\mathrm{d}\gamma/\mathrm{d}t)/(\mathrm{d}\gamma_0/\mathrm{d}t)]^\mathrm{M}\exp[-\lambda(T - T_\mathrm{ref})] \quad (23)$$

in which τ_0, γ_0, N, $\mathrm{d}\gamma_0/\mathrm{d}t$, M and λ are experimental constants. For this case, an alternative description of the strain rate dependence on strain rate is given as follows (*see* equation (12))

$$1/M = d\ln(\mathrm{d}\gamma/\mathrm{d}t)/d\ln\tau = \tau V^*/k_\mathrm{B}T \quad (24)$$

An interesting evaluation of equation (24) was made by Reed *et al.*[107] for the strain dependence of niobium single crystals for which with V^* being characteristically independent of strain for the bcc case, $1/M$ was shown to follow the same strain dependence as τ. The result argues for V^* having greater physical significance than M. And, further in the direction of developing a detailed TASRA based dislocation mechanics description of plastic flow is the mechanical threshold stress (MTS) model of Follansbee and Kocks[108] for the rate dependence of plastic flow also including history effects through evolution of the dislocation structure during plastic straining, as mentioned above for Klepaczko.[82] The MTS relation may be expressed in one way

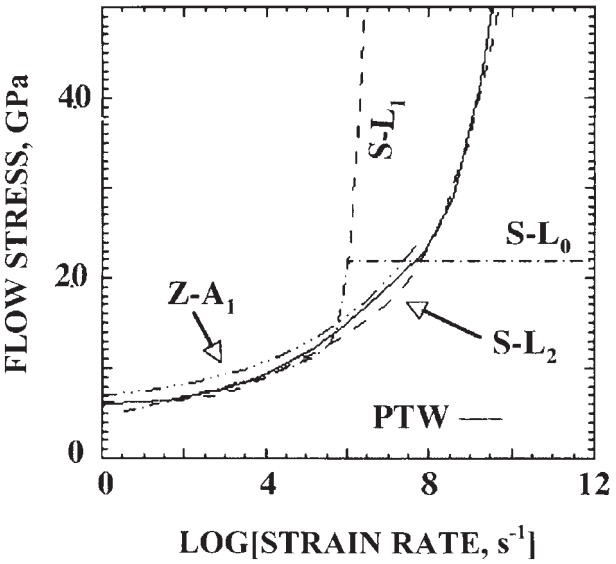

14 Predictions for flow stresses of tantalum at 50 GPa, 500 K and 0·1 plastic strain *v.* log strain rate for variety of constitutive models: Steinberg–Lund relation is shown in several modifications as S-L$_0$, S-L$_1$ and S-L$_2$; PTW is for Preston–Tonks–Wallace and Z–A$_1$ is bcc Zerilli–Armstrong equation, as adapted from results reported by Remington *et al.*[113]

$$\sigma = \sigma_\mathrm{a} + \left[1 - \left(\frac{k_\mathrm{B}T}{g_0 G b^3}\ln\frac{\mathrm{d}\varepsilon_0/\mathrm{d}t}{\mathrm{d}\varepsilon/\mathrm{d}t}\right)^{1/\mathrm{p}}\right]^{1/\mathrm{q}} + \sigma_\varepsilon\{T,(\mathrm{d}\varepsilon/\mathrm{d}t),\sigma\} \quad (25)$$

in which g_0, $\mathrm{d}\varepsilon_0/\mathrm{d}t$, p and q are experimental constants and $\sigma_\varepsilon\{T,(\mathrm{d}\varepsilon/\mathrm{d}t),\sigma\}$ represents the stress affected dislocation density evolution during straining. Gray, III *et al.*[109] have applied the analysis to the grain size dependent stress–strain behaviour of the fcc alloy Monel 400 extending from conventional to SHPB strain rates and for which a reasonably constant k_ε of ~17 MPa mm$^{1/2}$ was determined. Holmedal[110] has recently reviewed the MTS model. Among other model relations that have been developed particularly for high strain rate behaviours are ones by Steinberg *et al.*[111] and Bodner and Partom.[112] Remington *et al.*[113] have reviewed recently the testing conditions and constitutive equation applications at the highest rates of strain (*see* Fig. 14). The latter assessment connects also with model constitutive relations being developed with the method of molecular dynamics as made possible by the increase in capacity of modern computing machines. Examples in this category are provided, for example by Germann *et al.*,[114] by Kadau *et al.*,[115] by Lebensohn *et al.*[116] and by Caro *et al.*[117] Figure 15 is a Voronoi construction of 190 785 atoms from Kadau *et al.* These authors covered other simulated constructions that were achieved by sintering spherical nanoparticles of different sizes under prescribed temperature and pressure conditions. In both cases, periodic boundaries were employed. An interesting aspect of the small grain size regime, say, $\leqslant 10$ nm, investigated by Kadau *et al.* and relating to the discussion following equation (20) above, is that the strength of the simulated material was lower as the grain

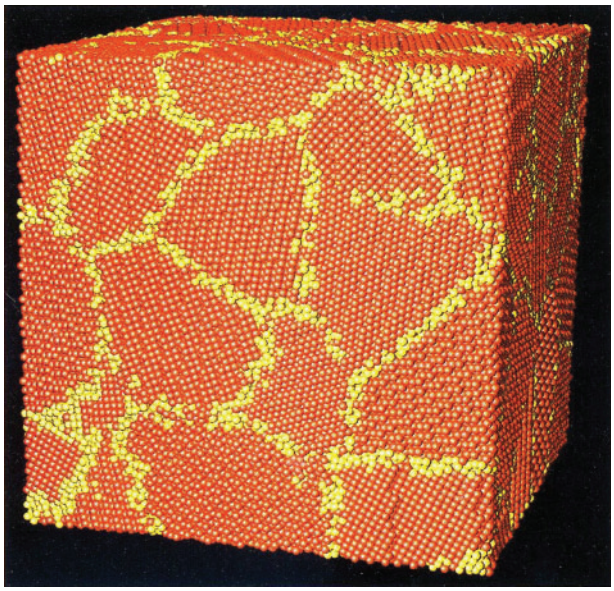

15 Molecular dynamics model of nanocrystalline aluminium material exhibiting grain size dependent reversal of flow stress at grain sizes below ~10 nm, that is, smaller grain size material is found to be weaker, as reported by Kadau *et al.*[115]

size was smaller. Rodriguez and Armstrong[118] have pointed out that for this limiting smallest grain size weakening condition, the SRS should also have to show a reversal based on models of such strain rate dependence. Argon and Yip[119] have modelled the transition from grain size strengthening to weakening as a method of achieving a 'strongest size' for a nanopolycrystalline aggregate.

High strain rate dependent material properties

Examples where imposed strain rates play an important role in determining material property outcomes are: the ductile–brittle transition behaviour of steel and related bcc metals, the fracture toughness properties of materials, occurrence of adiabatic shear banding, material responses to ballistic impacts and shock or isentropic compression experiments, in the latter case involving shockless testing at uniform loading rates over nanosecond timescales.

Ductile–brittle transition and fracture toughness properties

At lower temperatures or higher strain rates, steel and related bcc metals and alloys show a relatively abrupt transition from ductile plastic yielding to brittle cleavage fracturing. Krafft *et al.*[120] characterised their own ductile–brittle transition temperature (DBTT) measurements made for a low carbon steel material in terms of a shift in the material strain hardening behaviour produced by rapid plastic deformation. Charpy[7] V notch test results were also presented for comparison with tensile test measurements obtained over a range of strain rates. References were made to the prior investigations of Taylor[42] and von Karman and Duwez[52] concerning the propagation of plastic straining. Near to the time of Krafft *et al.*'s report, Cottrell[121] and Petch[122] also reported the results of their researches on a dislocation

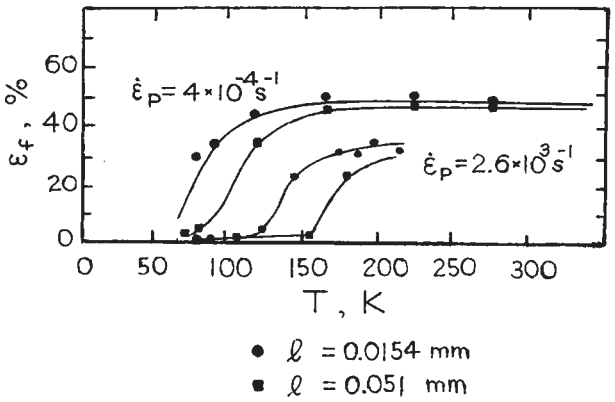

16 Tensile fracture strains as function of temperature for En2A mild steel material tested at two grain diameters l (● l=0·0154 mm, ■ l=0·051 mm) and at two plastic strain rates, as adapted from results reported by Campbell *et al.*[123]

mechanics based analysis of conditions for plasticity induced cracking at the DBTT and its dependence on testing method and material microstructural parameters. Figure 16 shows results obtained in tensile conventional and SHPB tests of a steel material, at two grain sizes, by Campbell *et al.*[123] The ductile–brittle transition is shown to be raised to higher temperature at the greater SHPB strain rate and for the larger polycrystal grain size. Rosenfield *et al.*[124] have reviewed the DBTT behaviour by placing emphasis on the sudden change produced in the material ductility.

Armstrong[125] has reviewed the dislocation mechanics basis for predicting the DBTT behaviour. The transition temperature T_c in a Charpy V notch test was specified by equating the cleavage fracture stress σ_c and the temperature and strain rate dependent yield stress σ_y, subject to plastic constraint at the V notch through the notch constraint factor α', as discussed by Orowan,[15] in the relationship

$$\sigma_c = \alpha' \sigma_y \{T, (d\varepsilon/dt)\} \tag{26}$$

With incorporation of the stress dependences on microstructural parameters, particularly the grain size dependence, an explicit equation for T_C was obtained as

$$T_c = (1/\beta) \left\{ \ln(\alpha' B) - \ln\left[(k_c - \alpha' k_y) + (\sigma_{0c} - \alpha' \sigma_G) l^{1/2} \right] - \ln l^{-1/2} \right\} \tag{27}$$

where k_c and k_y are the microstructural stress intensities for cleavage and yielding respectively, σ_{0c} is the relatively low friction stress for cleavage and the remaining parameters have been defined in equations (13)–(15). The equation compares favourably with the model equations proposed separately by Cottrell[121] and Petch.[122] Equation (27) was applied by Armstrong *et al.*[126] to evaluating very complete measurements that had been reported by Sandstrom and Bergstrom[127] for the ductile–brittle transition properties of a mild steel material, as shown in Fig. 17. For example, Sandstrom and Bergstrom had determined in their investigation that $\alpha' = 1{\cdot}94$ and that an effective strain rate of 400 s^{-1} was operative for their instrumented Charpy V notch test results. In Fig. 17, the DBTT is seen to be lowered by grain size refinement to an extent determined by how

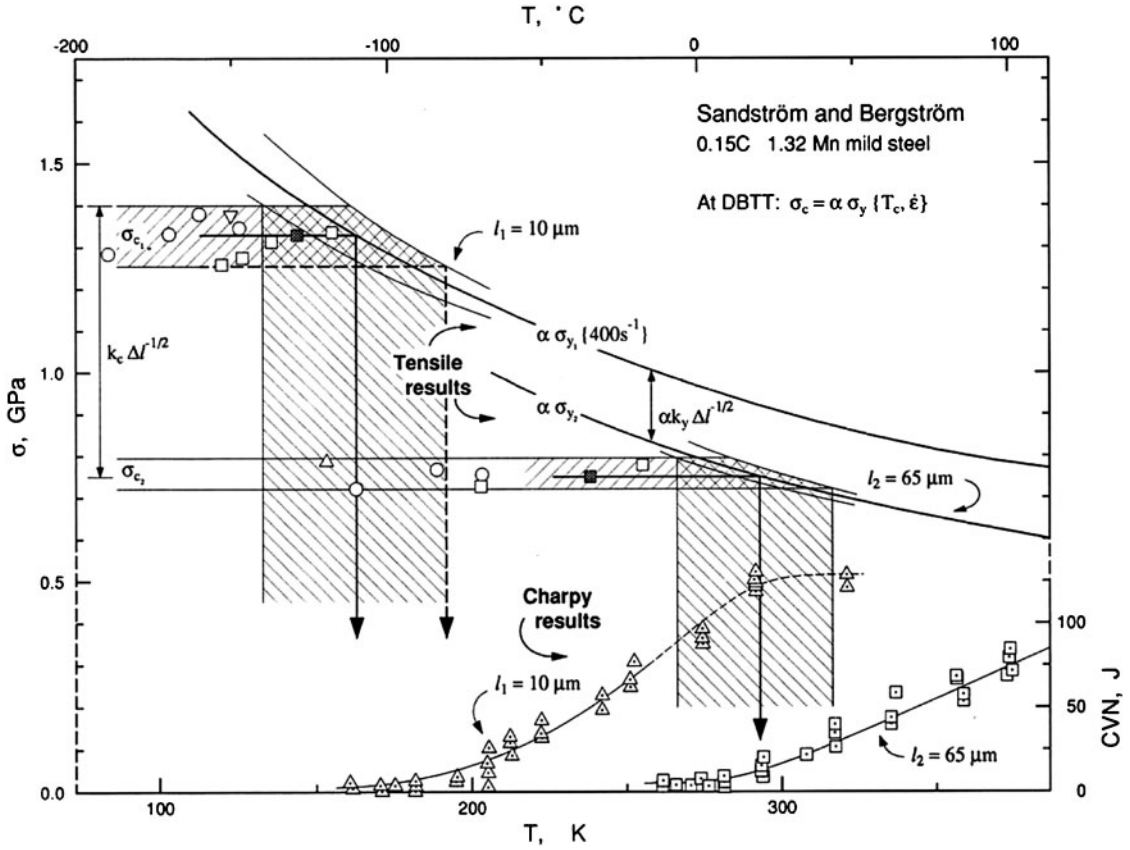

17 Connection of experimental tensile yield, cleavage fracture and Charpy V notch measurements with prediction of ductile–brittle transition behaviours for mild steel material as function of temperature at two grain diameters and taking into account notch constraint factor and effective strain rate for Charpy V notch tests, as adapted from results reported by Armstrong *et al.*[126]

much greater k_c is than k_y. The predicted DBTT for the smaller grain size material was proposed to be somewhat lower than the measured value in the Charpy V notch test because of the reported presence of larger brittle carbide particles.

Investigation of the influence of precracking on the static and dynamic fracturing properties of steel and related materials has led in a major way to the development of standardised 'fracture mechanics' test programmes, in continuation of the pioneering researches of Irwin[128,129] and colleagues. The microstructural stress intensity k_c is the counterpart of the stress intensity K_C measurement in fracture mechanics. Toth *et al.*[8] credit Kalthoff[130] with developing the fracture mechanics concept of dynamic impact response curves and their connection with impact fracture toughness measurements. A continuing research activity is to connect the microstructural aspects of fracturing with macroscopic engineering performances, for example, as investigated by Pisarenko *et al.*[131] who have provided an estimation of the fracture toughness dependence on temperature and strain rate. The researches have important consequences for control of neutron irradiation embrittlement in the nuclear power industries, as was the case for the initial investigations of Cottrell[121] and Petch[122] and as was true for later reviews provided both by Wechsler[132] and by Landes,[133] both giving emphases to testing standards and in the latter case, drawing attention to the comparison of static and dynamic fracture toughness measurements, as shown in Fig. 18. Petch and Armstrong[134] have provided the

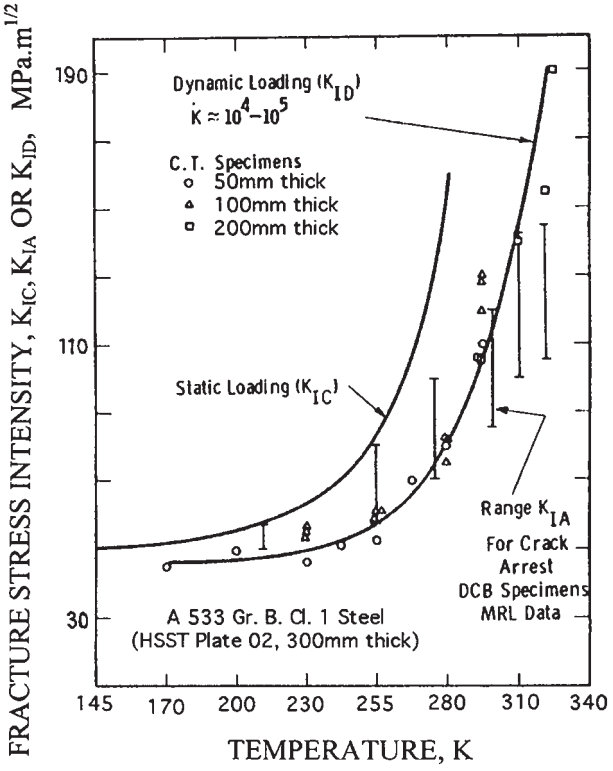

18 Temperature dependence of static K_{IC}, dynamic K_{ID} and crack arrest K_{IA} fracture toughness measurements for A533B Grade B Class1 nuclear pressure vessel steel, as adapted from results reported by Landes[133]

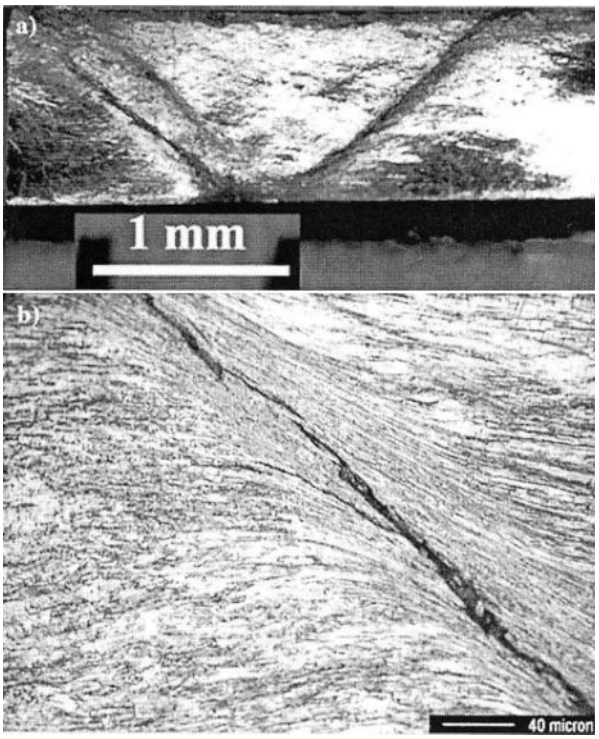

19 Adiabatic shear bands in ultrafine grain tungsten material *a* after uniaxial dynamic compression and *b* within shear band as revealed by polishing and etching, as reported by Wei[140]

following description to differentiate among the many microstructural factors that raise the yield strength of a material and more often than not, decrease its fracture toughness. Consider in the fracture toughness test that the load increases at the crack tip until plastic flow commences and strain hardening of the material builds up until cracking occurs and leads to material failure. Most microstructural strengthening mechanisms in steel raise the yield stress without significantly affecting the material strain hardening nor the fracture stress; thus, a smaller amount of strain hardening is required to reach the fracture stress and the material toughness decreases. This applies as well for the influence of greater strain rates and lower temperatures. However, although reduction in the grain size of a material increases the yield stress too, the grain size reduction increases more so the fracture stress, in accordance with $k_c > k_y$ as discussed above, and hence, the fracture toughness, is increased by the grain size refinement.

Adiabatic shear banding

In the preceding description, the microstructural stress intensity determined from the polycrystal grain size dependence, carrying on from equation (14), is an important parameter that is proposed to characterise localised material deformation behaviours in the polycrystal grain boundary regions. As will be seen, the same consideration comes into play for grain size determined aspects of adiabatic shear banding. But first, among others, Rogers[135] and Timothy[136] have produced important reviews of shear banding behaviours and recently, Walley[137] has produced an historical review of the subject. Extensive experimental and model results are produced in the monograph by Bai and Dodd.[138] The symposium proceedings edited by Armstrong *et al.*[139]

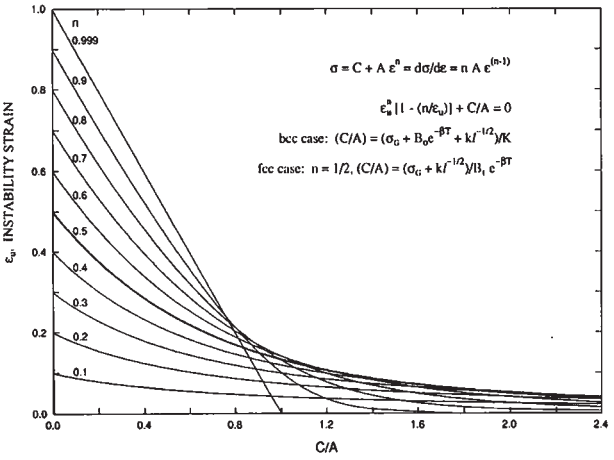

20 Considère tensile instability strain as function of strain hardening index, grain size and TASRA parameters for bcc and fcc metals, as adapted from results reported by Armstrong and Zerilli:[141] in figure legend, $A = K$ (for bcc case)

leads off with an important review by Gilman on historical aspects of the micromechanics of shear banding and especially, includes reference to the pioneering etch pit studies done with Johnston. A recent example of shear banding reported by Wei[140] for nanopolycrystalline tungsten material is shown in Fig. 19. The figure appears quite similar to that attributed to sketches of Tresca by Johnson.[10] Considère's equation (1), given above, has most often provided a starting point for evaluations of the behaviour. Armstrong and Zerilli[141] developed Fig. 20 on a Considère basis to differentiate in one way between the relative sensitivities of bcc and fcc materials to exhibiting shear banding behaviour. In the figure legend, the strain hardening behaviours for both structure types have been approximated by so called power law hardening (*see* equations (13)–(15)), in which case the strain exponent n is equal to the uniform strain at the maximum load point so long as the total stress is taken as a single quantity dependent on the strain. For the more complicated flow stress dependence, the uniform strain to the maximum load point ε_u is shown in the figure to be a function of the ratio C/A that increases at lower temperature and higher strain rates for the bcc case, hence producing a reduction in uniform strain corresponding to the maximum load point of Fig. 1 moving to smaller strains. Perhaps surprisingly, the opposite influence occurs for the fcc case in that C/A decreases at lower temperature and increasing strain rate, so leading to an increase in ε_u, and the maximum load point moves to larger strains. On the foregoing basis, fcc metals and alloys should be regarded as being less sensitive to exhibiting shear banding than bcc ones and this seems to be generally the case, for example, as listed in measurements compiled by Petch and Armstrong.[142] Voyiadjis and Abed[143] have provided finite element simulations for describing instability strains and strain localisation for the bcc metals tantalum, niobium and vanadium; and a more recent report[144] was extended to consideration of both bcc and fcc metal structures. The otherwise very useful Johnson–Cook equation (22) gives no effect of the strain rate on the maximum load point.

More detailed model analyses of the potential onset of shear banding behaviour have built onto the original

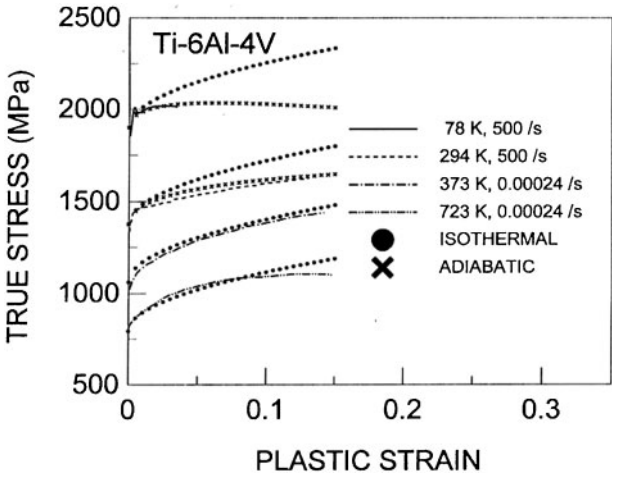

21 Isothermal and adiabatic Z–A descriptions of stress–strain curve for Ti–6Al–4V alloy tested at different temperatures and strain rates, as reported by Zerilli and Armstrong[77]

analysis of Zener and Hollomon[41] who gave emphasis to the importance of localised heating and the material strain hardening in determining the behaviour. Kubin *et al.*[145] developed a computer model to explain the enhancement of shear banding at lower test temperatures. Marchand and Duffy[146] reported the results for shear banding occurring in steel in a Hopkinson torsion bar. Important results for tantalum materials have been reported by Meyers *et al.*[147,148] Wright[149] has provided a shear band susceptibility relation containing the (power law) strain rate exponent M; *see* equation (23) and the reference to Nemat-Nasser *et al.*[106] Nesterenko[150] has provided an analysis based on continuum mechanics. Nesterenko points out that analysis of the self-organisation within a shear band pattern, reflecting the collective behaviour of the individual bands, provides an important test for proposed constitutive equations. Batra and Chen[151] had earlier investigated the relationship of the several strains for plastic instability, shear band initiation and minimum shear band spacing. In this same regard, Rabczuk *et al.*[152] have reported recently a mesh free sheared particle method of modelling shear band structures. The strain rate dependence was modelled with the Johnson–Cook[103,104] equation (22). In addition to assessment of results on explosively collapsed cylinder shear band structures described in experiments of Nesterenko with colleagues, added analysis is provided on a shear band basis of the brittle fracture to ductile shear banding behaviours investigated by Kalthoff.[130] Figure 21, taken from Zerilli and Armstrong,[74] shows an influence of isothermal and adiabatic temperature conditions on modelling of the stress–strain behaviour of shear band prone Ti–6Al–4V alloy material that is known to have a relatively low thermal conductivity. In further work, Zerilli and Armstrong[153] have provided an assessment of the relationship for the onset of shear banding, attributed to Bai and Dodd[138]

$$-\tau_0(\partial\tau/\partial T)_0/\rho_0 c_v(\partial\tau/\partial\gamma_0) \geqslant 1+\left[4\kappa(\mathrm{d}\gamma/\mathrm{d}t)(\partial\tau/\partial T)_0/\rho_0 c_v^2(\partial\tau/\partial\gamma)_0\right]^{1/2} \quad (28)$$

and noted that although the trend predicted for material behaviour was in the correct direction, the onset of shear banding fell short of quantitative prediction.

An alternative consideration put forward for the origin of adiabatic shear banding was that it should have to be explained at the more fundamental level of dislocation pile-up avalanches associated with strong microstructural obstacle collapses, as estimated by Armstrong *et al.*[154] for localised 'hot spot' heating behaviour causing explosive chemical decompositions. Figure 22 illustrates for a number of metals and alloys a graphical procedure that was proposed for assessing the consequent shear banding susceptibility on a further extension of the dislocation pile-up avalanche model basis proposed by Armstrong and Elban.[155] The inset relation in the figure applies for a theoretically overestimated temperature rise for pile-up collapse. The main material variables are the upper limiting microstructural shear stress intensity for cracking k_s that is plotted *v.* the material thermal conductivity. A greater susceptibility to shear banding is indicated by an increasing slope of the ordinate line to any plotted material point. More recently, Armstrong and Grise[156] have reported relatively lower temperature rises, but still substantial ones, for numerically modelled pile-up avalanches involving only a few dislocations. The numerical simulations serve as well to provide quantitative validation of the model proposal. In Fig. 22, in agreement with experiment, bcc metals are indicated to be far more susceptible than fcc ones and a greater susceptibility is indicated for α-Ti and even more so for Ti–6Al–4V alloy.

Ballistic impacts

The susceptibility of α-Ti to shear band formation was demonstrated in high strain rate loading of a 'hat shaped' specimen employed in conventional compression and Hopkinson bar experiments reported by Meyers *et al.*[157] The test set-up had been utilised previously by Hartmann *et al.*[158] For the α-Ti experiments, the Johnson–Cook[103,104] constitutive equation (22) (*see* above) was employed to estimate the temperature rises generated in the sheared circumferential edges of the hat shaped specimen. Also, Holt *et al.*[159] conducted gas gun propelled punch tests of discs of Ti–6Al–4V alloy launched onto a hardened steel rod material and observed substantial shear bands to have propagated into the target from the circumferential wall of the cratered alloy. At the highest impact velocities, melted alloy material was sprayed onto the exposed surface of the punch. More recently, Martinez *et al.*[160] studied the microstructures produced in similarly plugged materials of the same type, but thicker plate, Ti–6Al–4V alloy by direct gun launching of steel projectiles at higher velocities. Magness, Jr[161] provided a comprehensive description of more conventional, higher density, tungsten and uranium alloy penetrator materials and penetrated targets.

Zernow and Chapyak[162] reported on melting associated with shear band formation within a molybdenum shaped charge slug. Copper, iron and tantalum explosively formed projectiles (EFP) produced by detonated liner materials were extensively studied by Pappu and Murr[163] for the purpose of investigating the deformed material microstructures and especially, to assess the Zerilli–Armstrong[72,75] (Z–A) and Johnson–Cook[103,104] (J–C) constitutive relations for modelling the deformed

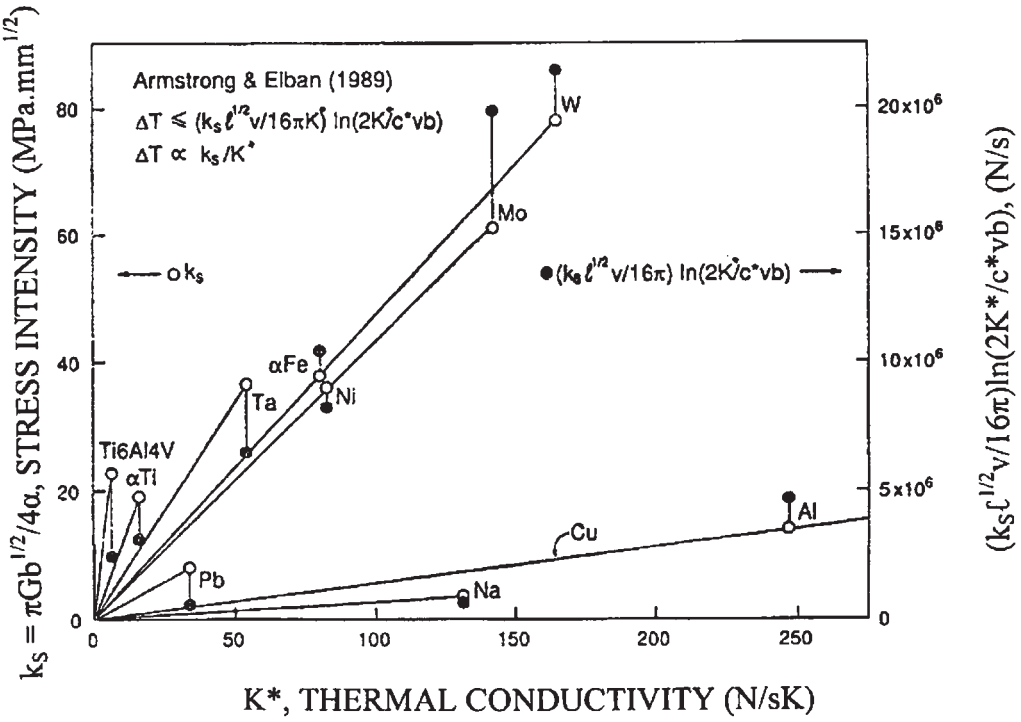

22 Susceptibility to shear banding on dislocation pile-up avalanche basis,[155] as adapted from results reported by Armstrong and Zerilli:[141] in internal figure legend, ΔT is upper estimate of temperature rise, k_s is microstructural shear stress intensity for cracking, K^* is thermal conductivity, v is shear wave speed and c^* is specific heat at constant volume

specimen shapes. Figure 23 is an illustration of two computed EFP shapes and their residual stress profiles which were obtained for two tantalum materials characterised with different Z–A parameters and employing the Autodyn-2D hydrocode. Microstructural analyses of the recovered materials were made by optical and transmission electron microscopy (TEM). It was concluded that dynamic recovery was relatively important to the results obtained on tantalum in comparison with complete recrystallisation occurring during the deformation of copper, and for iron, extensive twinning was important to the occurrence of dynamic recrystallisation and the development of shear banding. Nevertheless, reasonably accurate modelling results were obtained with both the Z–A and J–C equations. In a companion investigation, Kennedy and Murr[164] employed the Autodyn-2D hydrocode with Z–A and J–C equations utilised to describe experimental results obtained on the complete penetration of copper and aluminium 7039 alloy target materials with tungsten heavy alloy (WHA) penetrators. Satisfactory modelling results were obtained and, again excellent optical and TEM micrographs were presented. In an investigation of the partial penetration of thick aluminium target plates, Valerio-Flores *et al.*[165] reported light microscopy, scanning electron microscopy and TEM results of the cratered material. Also, hardening of the material was illustrated via axial hardness measurements made ahead of the point of peak penetration on longitudinal sections of the cratered material; and the results were modelled with the Autodyn-2D hydrocode employing the J-C equations. Single crystal tungsten rod penetrators were employed by Pizana *et al.*[166] for study of rod erosion in the process of cratering steel targets. Dey *et al.*[167] have recently presented a comprehensive study of numerical simulations of thick Weldex E steel plates subjected to perforation by Arne tool steel impactors. Both Z–A and J–C constitutive relations, in the latter case including a fracture criterion, were employed, after equation

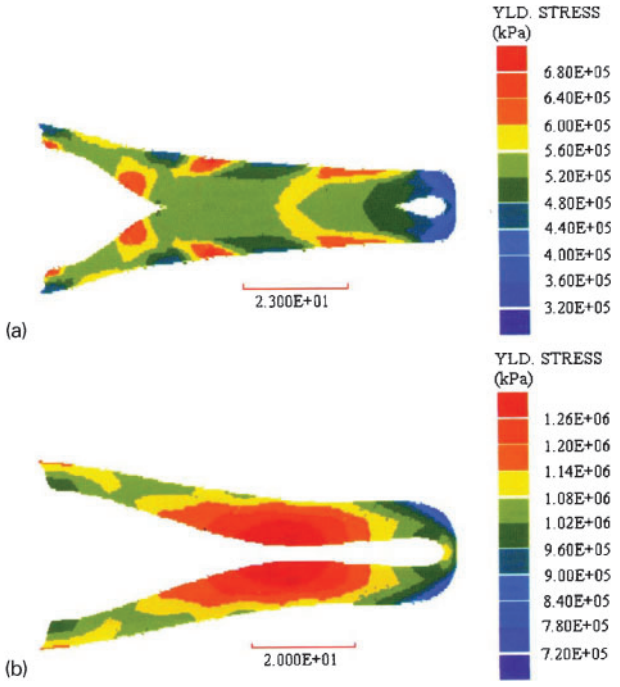

23 Comparison of EFP shapes and residual 'yield stress' profiles computed for two Ta materials modelled with Zerilli–Armstrong[75] constitutive relationship and employing equation parameters determined from separate reference tests, as adapted from results reported by Pappu and Murr[163]

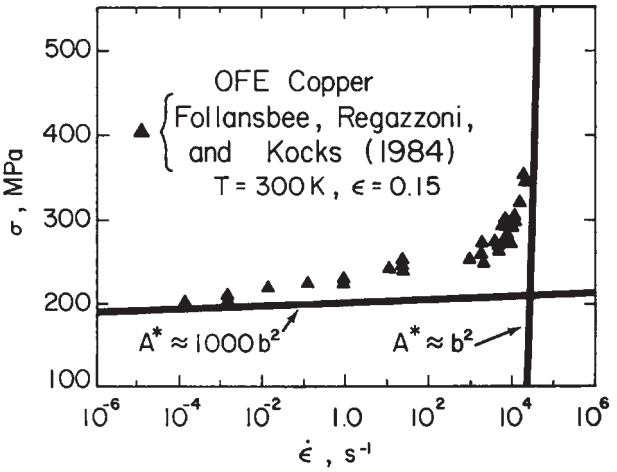

24 Thermal activation–strain rate analysis activation area asymptotes applied to measurements of Follansbee *et al.*[174] reported for copper of flow stress dependence on strain rate[175]

validation experiments, with the LS-Dyna hydrocode to satisfactorily model the results.

Shock and ICE results

Shock wave phenomena, obtained at loading pressures greater than those associated with SHPB studies, have been modelled hydrodynamically to involve discontinuities in pressure, temperature and density across an idealised shock front of negligible thickness. McQueen *et al.*[168] have reported on the equation of state (EOS) studies achieved under shock loading as related to essentially static high pressure measurements. Smith[169] reported in a pioneering study published in 1958 on the hardening of metals produced by shock wave loading. Smith presented a model for dislocation creation at the shock front. Publications by Weertman and Follansbee,[170] Gray, III[171] and Bringa *et al.*[172] are representative examples of progress made by model developments to describe the shock induced plasticity of metals and alloys. Latest results both on EOS studies and many aspects of shock induced plasticity are reported in the biennial (odd year) American Institute of Physics Conference Proceedings series 'Shock compression of condensed matter – XXXX'; *see*, for example, Ref. 16 and the report by Jensen *et al.*[173] on the polymorphic bcc to hcp phase transformation in iron single crystals under quasi-isentropic loading and in plate impact tests.

At the high strain rate end of SHPB measurements made on copper, Follansbee *et al.*[174] had reported an important upturn in the flow stress dependence on strain rate as reproduced in Fig. 24 that was adapted by Armstrong *et al.*[175] to show relationship to the limiting values of the TASRA based parameter A^* (*see* equation (12)). At the lower strain rates shown in the figure, reasonable fit was obtained with the Z–A equation (13) employing constants determined from other measurements.[72] As shown in the figure, the high end of the SHPB strain rate measurements indicate transition to a lower limiting value of the dislocation activation area $A^* \sim b^2$. Also, in this high strain rate regime, it was pointed out that an increase in the material ductility had occurred and this was inconsistent with control by a dislocation drag mechanism that had been earlier

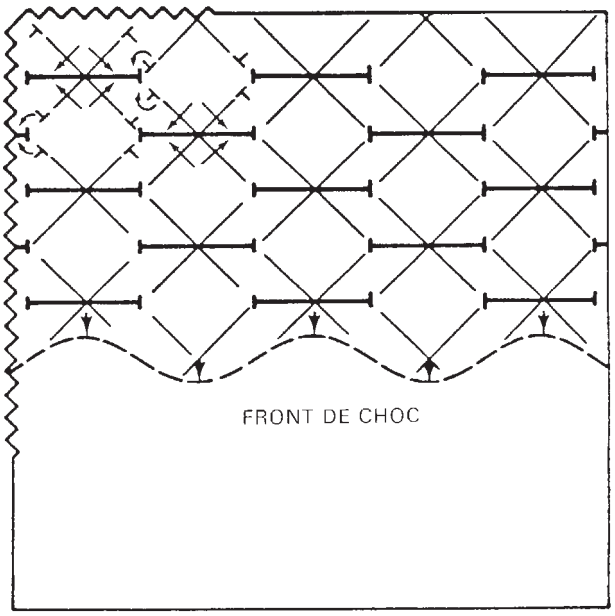

25 Residual dislocation dipole structure, representing essentially one-dimensional state of strain, proposed to be formed sequentially at nanoscale dimensions along direction of propagating shock, as reported by Armstrong[183]

thought to apply for the measurements.[53,175] Rather, it was proposed in further research of the dislocation drag consideration by Zerilli and Armstrong[176] that control of the strain rate was being taken over by a new mechanism of dislocation generation. Support for the dislocation generation mechanism has been provided very recently by connection of the measurements with shock induced plasticity measurements, as to be described below. More recently, Gray, III *et al.*[177] have reported on the influence of a reduction in grain size also increasing the ductility of copper in dynamic extrusion tests modelled with the Mesa hydrocode. Armstrong[178] has described an important influence of grain size on the true ductile fracture stress and consequent true fracture strain.

For the shock case, as mentioned above, a one-dimensional state of strain is taken to apply in the direction of shock propagation. Meyers[179] added to the Smith[169] model for dislocation generation at a propagating shock front by modelling the progressive formation of a repetitive structure during passage of the shock. Shehadeh *et al.*[180,181] have produced model calculations of high rates of dislocation multiplication occurring in copper and aluminium crystals at Orowan type velocity controlled strain rates in the range of 10^5–10^7 s^{-1}. In further simulation work, Shehadeh *et al.*[182] added the consideration of homogeneous dislocation nucleations occurring at relatively higher shock pressures. In any case, the shock front is imagined to be a narrow zone of nanoscale dimensions experiencing shear stresses near to the theoretical limit for dislocation generation.

Figure 25 shows another model[183] proposed for an idealised shock induced dislocation structure that conforms to a residual state of one-dimensional strain. Bandak and colleagues[184–186] have described various details of the model. Recently, the model has been associated by Armstrong *et al.*[187] with the nanoscale dislocation generation mechanism proposed to be

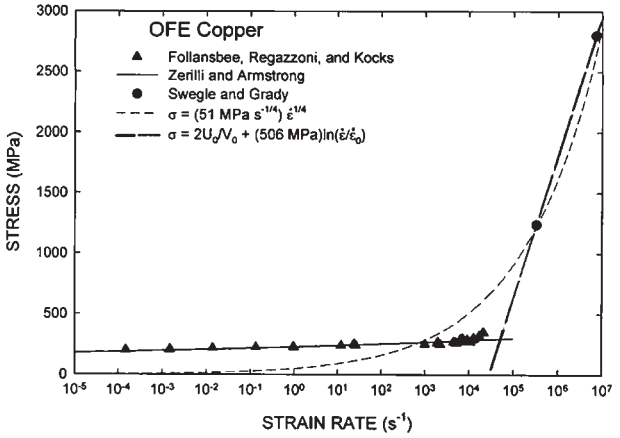

26 Flow stress of polycrystalline OFE copper determined over wide range of strain rates indicating transition from constitutive behaviour controlled by dislocation mobility to that of shock control by dislocation generation, as reported by Armstrong *et al.*[187]

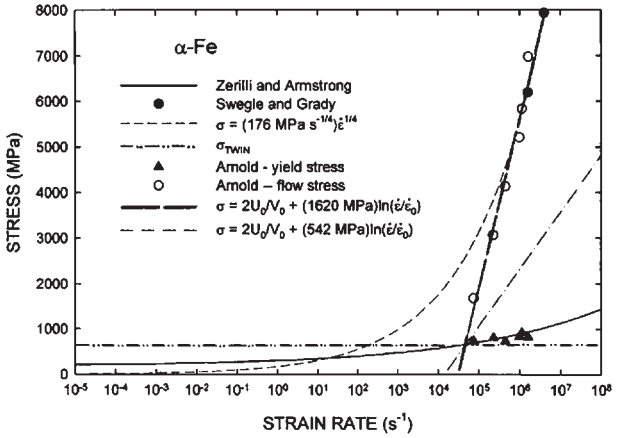

27 Flow stress of polycrystalline Armco iron material determined over wide range of strain rates indicating transition from constitutive behaviour determined by dislocation mobility to that of shock control by deformation twin generation, as reported by Armstrong *et al.*[187]

signalled at the upturn in the copper SHPB measurements shown in Fig. 24; and further, that such upturn establishes connection also with pioneering shock induced plasticity results reported for copper and other materials by Swegle and Grady.[188] Figure 26 shows adaptation on the same stress *v.* log strain rate scale of the previous measurements reported by Follansbee *et al.*[174] and those measurements for copper reported by Swegle and Grady. The lower strain rate measurements are shown in relation to the Z–A equation description; and in this case, the shock induced plasticity measurements are shown in relation to an empirical power law dependence proposed by Swegle and Grady and also, a model dislocation generation equation, at limiting small activation volume, developed by Armstrong *et al.*[187] as

$$\sigma = \left(2G_{0G}/V^*_{0G}\right) - \left(2k_B T/V^*_{0G}\right)\ln\left[(\mathrm{d}\varepsilon/\mathrm{d}t)_{0G}/(\mathrm{d}\varepsilon/\mathrm{d}t)\right] \quad (29)$$

In equation (29), that builds onto the companion equation (5) rather than equation (4) from Orowan, G_{0G} is the reference Gibbs free energy for dislocation creation in the absence of stress, V_{0G}* is the limiting small activation volume for slip and $(\mathrm{d}\varepsilon/\mathrm{d}t)_{0G}$ is the reference upper limiting strain rate. The quantity $2G_{0G}/V_{0G}$*) is the stress for dislocation generation in the absence of thermal activation. Very recently, Zhu *et al.*[189] have reported an essentially identical equation to that of equation (29) for the modelled surface nucleation of dislocations in deformation of dislocation free nanopillars; *see* also related results reported by Tschopp and McDowell.[190]

A similar assessment was made by Armstrong *et al.*[187] of the relationship of the Swegle and Grady[188] results reported for iron in comparison both with the lower strain rate Z–A equation description and with shock induced plasticity results reported for Armco iron materials of different grain sizes by Arnold.[191] Arnold had attributed the shock induced plastic deformation to the onset of deformation twinning behaviour. Figure 27 shows comparison of the several features of: the lower strain rate Z–A relationship, the Arnold measurements that overlapped those reported by Swegle and Grady, a predicted value[73] for the deformation twinning stress and the fit of equation (29) to the shock induced plasticity results. In this case, a value of $V^*_{0G} = b^2_T b = b^3/3$ was obtained as the lower limiting value for a smallest twin nucleus. An analogous result to that for Armco iron was obtained for tantalum material results reported: at the lower strain rate end, by Hoge and Mukherjee,[85] for the occurrence of deformation twinning, by Murr *et al.*[192] and at the higher shock induced plasticity stress levels, by Meyers.[193] It is interesting, relative to lack of twinning concern for copper, that Cao *et al.*[194,195] observed deformation twinning stresses for copper single crystals at a Hugoniot pressure of 30 GPa for laser induced shocks and for both laser and (longer pulse) explosively driven plate impact shocks at 55–60 GPa, these values being far above earlier established twinning stress measurements.

In comparison with shock loading, the relatively more recent advent of shockless ICE results have led to higher plastic flow stresses, for example, as observed by Jarmakani *et al.*[196,197] in copper during uniform loading of specimens over a period of nanoseconds. Armstrong *et al.*[198] have proposed that the high stresses occur because the uniform build-up of straining leads to the relatively low residual dislocation density being required to 'carry the load' by moving at upper limiting, drag resisted, dislocation velocities. Figure 28 provides a comparison on a log/log scale of the Jarmakani *et al.* results and the discussed above results of Follansbee *et al.* and Swegle and Grady, also with the previous constitutive equation descriptions plus an added one for drag resistance incorporated into the Z–A equation.[176] For this case, the TASRA component of the Z–A flow stress equation is obtained in a drag modified form as

$$\sigma^* = m\tau = B\exp(-\beta T)/\left\{1 - [c(\mathrm{d}\varepsilon/\mathrm{d}t)/\beta_1\sigma^*]^{\beta_1 T}\right\} \quad (30)$$

where $c = c_0 m^2 \beta_1/\rho b^2$, c_0 is the drag coefficient and the other terms are previously defined in equations (4), (13) and (15). At an upper limiting dislocation velocity

$$\sigma^* = \left(m^2 c_0/\rho b^2\right)(\mathrm{d}\varepsilon/\mathrm{d}t) \quad (31)$$

that is a linear dependence of σ* obtains as shown in

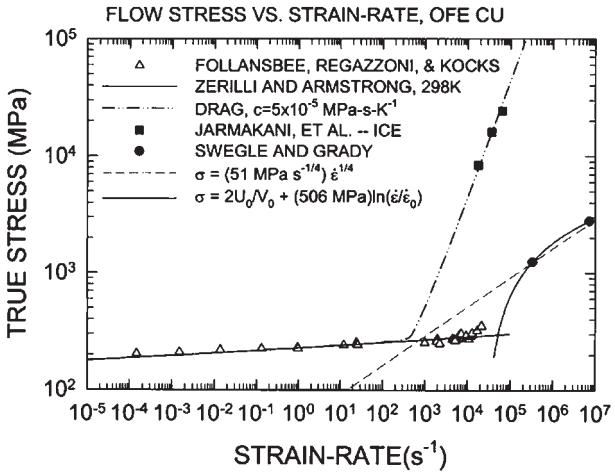

28 Conventional, SHPB, shock and ICE flow stress measurements plotted on log/log scale for copper and including Z–A type constitutive equation descriptions for two different strain rate dependences, as reported by Armstrong *et al.*[198]

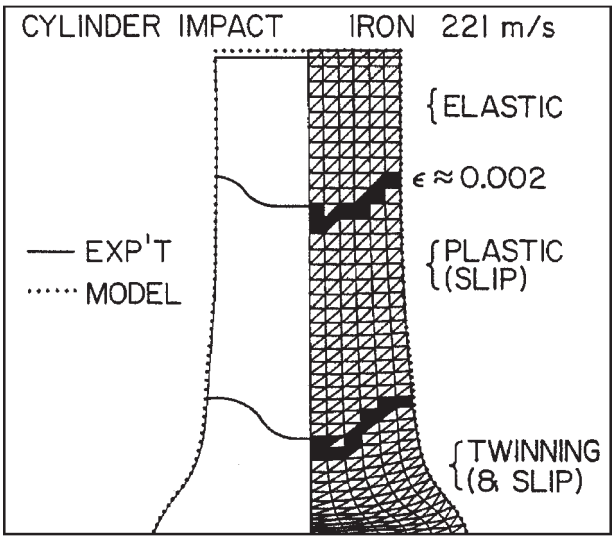

29 Measured[103,104] and computed longitudinal cross-section of Taylor solid cylinder impact specimen of iron having undergone deformation twinning on initial impact and afterwards, been deformed by follow-on slip, compared with Fig. 3, as reported by Zerilli and Armstrong[73]

Fig. 28. A value of $c=5\times10^{-5}$ MPa s K^{-1} is determined from the linear slope dependence and is consistent with a previous estimate for copper.[176] For SRS comparison, the flow stress dependence on the natural logarithm of strain rate is evaluated as

$$[\partial\sigma/\partial\ln(\mathrm{d}\varepsilon/\mathrm{d}t)]_T=\sigma \tag{32}$$

in which case a mean value of ~17·6 GPa is obtained, far greater than the 0·506 GPa value determined from equation (29) and shown in Fig. 26.

Metallographic and related observations

A considerable number of research investigations into the higher strain rate behaviours of metals and alloys have been conducted by employing conventional metallurgical practices in the evaluations of mostly post-deformation microstructures of the deformed materials and especially, at the highest strain rates involved in shock loading. As mentioned above, Field *et al.*[60] have reviewed a number of important techniques for making real time measurements. Remington *et al.*[113] provide a description of techniques applied under extremely high pressure conditions, including relation to the mentioned X-ray diffraction results achieved by Wark *et al.*[16] on a nanosecond timescale. Outstanding metallographic results have been reported beginning from the pioneering observations reported by Smith.[169] Such metallographic observations have been continued in many cases with addition of TEM observations, as reported above in the section on 'Ballistic impacts', for example, by Murr and colleagues[163 and 166].

Slip *v.* deformation twinning

Beginning from the earliest deformation twinning test results reported at higher strain rates for hcp magnesium by Barrett and Haller,[43] for fcc metals and alloys of low stacking fault energy by Murr and Esquivel[199] and for the pioneering Taylor test results on iron analysed by Carrington and Gayler,[46] there has been the issue of the conditions for conversion from slip to deformation twinning behaviours. The combination of twinning and slip results obtained in the original Taylor tests done on iron, as shown in Fig. 3 from Carrington and Gayler, was reproduced to great extent in later calculations performed by Zerilli and Armstrong,[73] as shown in Fig. 29; *see* also the article by Armstrong and Zerilli.[53] In the calculations, the stress for deformation twinning was taken to be essentially athermal but reasonably strongly dependent on the material grain size, in agreement with the stress–grain size relationship[200,201]

$$\sigma=\sigma_{0T}+k_T l^{-1/2} \tag{33}$$

for which σ_{0T} and k_T are experimental constants. For iron, the twinning k_T has a value only slightly below k_C and thus, twinning and cleavage fracture are often associated. Figure 30 shows experimental confirmation of equation (33) for a compilation of grain size dependent twinning stresses reported for iron. The Moiseev and Trefilov[202] results were obtained from SHPB tests at a strain rate of $1{\cdot}1\times10^3$ s^{-1}, and for which the determination of proportional limit stresses for twinning occurred at different temperatures in the range 88 to 248 K, and were higher as the material grain size was larger. At a reasonably small grain size in Fig. 30, both proportional limit and bulk yield stress values are shown from Madhava *et al.*[203] for a low carbon steel material tested in compression at liquid helium temperature. The solid line dependence for bulk yielding controlled by twinning, with $\sigma_{0T}=330$ MPa and $k_T=90$ MPa $mm^{1/2}$, was employed in the calculations leading to Fig. 29. Also in Fig. 30, the lesser dependence of yield stress on grain size is shown for equation (13) as computed on a slip controlled Z–A constitutive basis. The transition from slip to twinning is shown to occur at smaller grain size for higher strain rates, similar to the effect of lowering the test temperature.

To better understand the Taylor test result in Fig. 29, McKirgan[204] undertook a research effort to follow via sequential EPIC hydrocode modelling on a microsecond timescale with the Z–A and twinning relations the competition between twinning and slip during Taylor

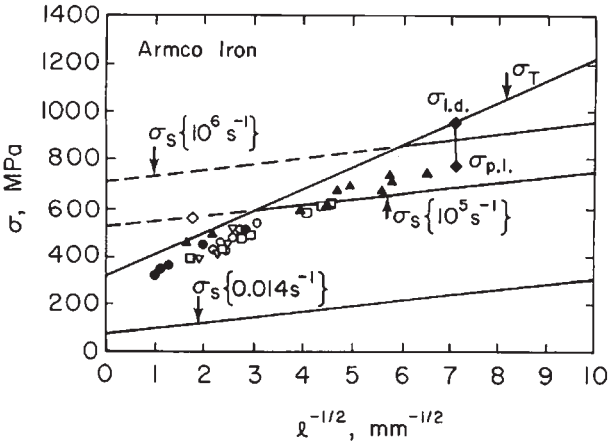

30 Dynamic SHPB proportional limit stress measurements for deformation twinning in different grain size Armco iron materials tested at different temperatures[202] and also, compressive proportional limit and bulk yield twinning stresses measured by conventional compression for low carbon steel material tested at liquid helium temperature,[203] both in comparison with estimation of deformation twinning stress dependences on grain size and slip stress dependences computed at different strain rates with bcc Z–A equation, as reported by Armstrong and Zerilli:[53] open diamond point, measured at strain rate of $10^5\ s^{-1}$, is from R. W. Rohde, 'Dynamic yield of shock-loaded iron from 76 to 573 K', *Acta Metall.*, 1969, 17, 353–363

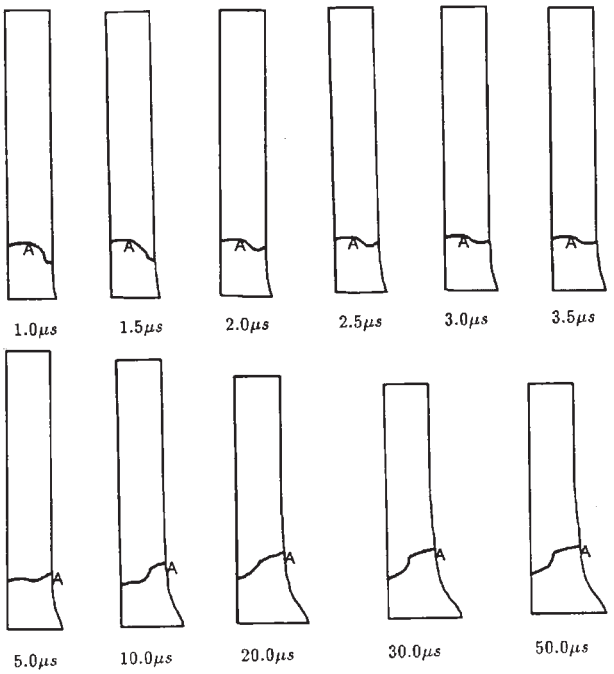

31 Sequential model computations, employing Z–A equation in EPIC on microsecond timescale, of 'limit' of deformation twinning, marked by boundary A, first having proceeded up cylinder axis on initial impact of Taylor type Armco iron cylinder and subsequently, in time moved downward through follow-on deformation by slip, as reported by McKirgan[204]

impact of the same iron material previously evaluated for constitutive equation constants by Johnson and Cook.[103,104] Figure 31 shows the sequence of results by which during impact, twinning first occurs at and behind the impact surface and is followed later by thermally activated slip. Of interest is the initial convex twinning interface that is reversed by follow-on slip to produce the eventual concave boundary analogous to that reported by Carrington and Gayler.[46] As mentioned above, Arnold[191] determined a controlling role for deformation twinning in determining the shock induced plasticity of his Armco iron materials via quantitative optical microscopy done on the recovered specimens. Other investigations bearing on deformation twinning behaviours under high strain rate conditions are reported as follows: Gray, III[205] for twinning in Al–4·8Mg alloy, and Murr *et al.*[206] and Lins *et al.*[207] for twinning connection with adiabatic shear banding.

Dynamic recrystallisation and spallation/fragmentation

A dependence on the extent of deformation (and temperature) of the solid state recrystallisation and grain growth properties of metals and alloys is indicated in Fig. 32 that was taken from the pioneering book co-authored by Schmid and Boas.[38] Conditions under high strain rate loading are much more complicated but the observational techniques for studying the behaviour have been greatly expanded. For example, Lins *et al.*,[207] whose researches on adiabatic shear banding were mentioned above, reported also in their investigation on 'progressive subgrain misorientation' recrystallisation occurring within the shear bands during SHPB testing of the interstitial free steel material. In the study, backscattered electron micrographs obtained with the scanning electron microscope and selected area diffraction patterns, along with orientation imaging microscopy, were employed to trace the development of new grain orientations. Xue *et al.*[208] employed TEM observations to describe the dynamic/static recovery and continuous dynamic recrystallisation behaviour within shear bands produced by the high rate shearing deformation of a cold rolled 316L stainless steel material. Yang *et al.*[209] have compared copper single crystal defect observations made with TEM on longer pulse, plate impacted, *v.* shorter pulse, laser shocked

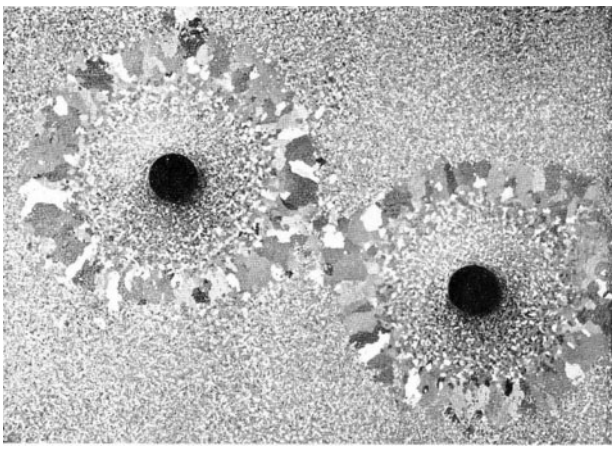

32 Influence of differing strains and thermal anneal on production of radially dependent recrystallised grain structure in region surrounding two bullet holes put through sheet of tin, as reported by Schmid and Boas[38]

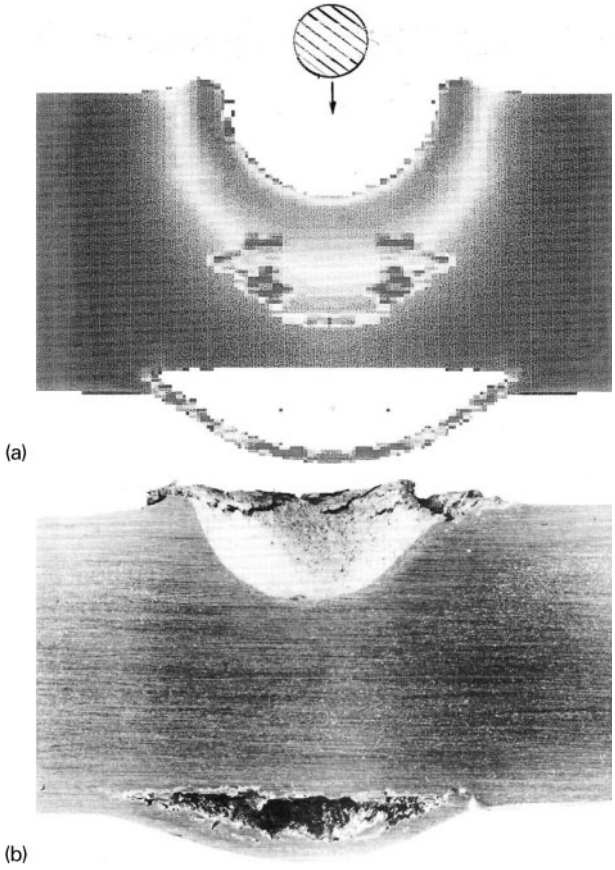

33 Comparison of *a* (3.-Eulerian) Autodyn modelled crater and *b* experimental measurement produced in copper by impacting of 3·18 mm diameter 1100 aluminium sphere at velocity of 6·01 km s^{-1}, as adapted from results reported by Quinones and Murr[213]

specimens. The J-C constitutive equation was employed to estimate temperature rises within the crystals. Esquivel and Murr[210] followed both the shock induced slip–twinning transition as it related to the onset of dynamic recrystallisation in plate impact tests of fcc metals such as nickel, copper, 70/30 brass and stainless steel alloys. An authoritative pictorial review of dynamic recrystallisation results for metals and alloys has been presented by Murr and Pizana.[211] The review gives an excellent historical description of both static and dynamic recrystallisations. The two behaviours are associated with quite different grain scales. Also, Medyanik *et al.*[212] have employed the onset of dynamic recrystallisation as a physical criterion for modelling adiabatic shear band propagations in 4340 steel alloy and oxygen free high conductivity (OFHC) copper. The different material thermal conductivities played a major role in determining the model estimations of shear band widths, propagation speeds and temperature rises, all of which were more localised for the 4340 steel material; *see* possible relation to the graphical results in Fig. 22.

Figure 33, taken from Quinones and Murr,[213] is a striking example of the modelled and experimental observation of spallation induced at the back surface of a 1·3 cm thick OFHC copper plate by gas gun propelled impact of a 3·18 mm diameter 1100 aluminium projectile. The projectile struck the plate at a velocity of 6·01 km s^{-1}. The impact was modelled on a microsecond timescale. The Autodyn 3·0 hydrocode employing the J-C constitutive equation was employed to model the experiment. Wells and Brannon[214] have reported on damage assessments made via X-ray computed tomography (XCT) applied to ballistic impacts. A pioneering reference for fragmentation and spallation results was reported by Seaman[215] and followed up with an article co-authored by Seamon with Curran and Shockey.[216] Beyond the plate impact experiments accomplished on Armco iron by Arnold having relative thicknesses designed to also study spallation, reference is supplied in the work to important results reported by Romanchenko and Stepanov.[217] Panov *et al.*[218] have employed DYNA3D and the MTS model[108] to provide, with simulation of results on OFHC copper, validation of a predictive model for spallation results in plate impact tests. An updated description of modelling considerations involved in fragmentation studies is given by Grady.[219] Brannon *et al.*[220] report also on the 'grand challenge' of modelling damage and brittle failures in armour type ceramics, with assistance of XCT and as investigated in a variety of test conditions including the production of spallation results.

Lastly, among the many techniques being applied to deciphering spallation and related results as part of the higher strain rate properties of metals and alloys are the more widely employed line imaging velocity interferometry system for any reflector (VISAR) technique and the relatively newer method of transient interferometric microscopy (TIM). Furnish *et al.*[221] have reported line imaging VISAR measurements characterising the microsecond determined collapse of an individual pore in copper. In like fashion, Furnish *et al.*[222] have reported a shock induced spall strength of tantalum material of ~7 GPa; *see* Ref. 192 for comparison. The aim of TIM is to observe via real time shock -induced plastic deformations at grain boundaries. Initial results have been described by Greenfield *et al.* in a recent series of articles.[223–225]

Summary

The high strain rate properties of metals and alloys have been reviewed with initial emphasis on historical developments beginning from the earliest reporting of load–elongation and stress–strain curves, thence leading to results obtained on various dynamic loadings achieved by Charpy type pendulum impacts, split Hopkinson pressure bar measurements, ballistic impacts, shock induced plasticity and isentropic compression experiments. The measurements have been interpreted mostly on a dislocation mechanics model basis that provides for significant property differences among fcc, bcc and hcp crystal lattice structures also spanning the range from single crystals to nanopolycrystals. Adiabatic shear banding is described for higher strain rate deformations. In addition, the conversion of slip controlled plasticity to deformation twinning is assessed. At the highest strain rates associated with shocks, transition occurs from plasticity controlled by dislocation or twinning defect movements to control by slip or twinning defect generations. Such shock behaviour differs from the shockless uniform loading of an ICE where the original dislocation density is required to 'carry the load' by moving at upper limiting, drag resisted velocities. Important material property descriptions are given for the strain rate (and temperature)

dependent ductile to brittle transition behaviour of steel and related materials and of the ballistic impact behaviours of a wider range of metals and alloys. Challenging observations made via X-ray diffraction, metallographic, electron microscope and optical VISAR and TIM techniques have assisted greatly in establishing the current state of knowledge.

Added note: G. M. Owolabi, A. G. Odeshi, M. N. K. Singh and M. N. Bassim report in 'Dynamic shear band formation in aluminum 6061-T6 and aluminum 6061-T6/Al_2O_3 composites', *Mater. Sci. Eng. A*, 2007, **A457**, 114–119, that adiabatic shear banding was promoted in high velocity impacts by the Al_2O_3 particulate strengthening. Such strengthening and associated cracking promoted by the particles may relate to the dislocation pile-up avalanche model for shear band susceptibility described here in Fig. 22.

Acknowledgements

One of the authors, S. M. Walley, thanks Professor B. Dodd for comments received at the beginning of development of the present article. Professor H. Conrad is thanked for assistance in tracking the Schmid and Boas (Figs. 2 and 32). Professor L. Murr is thanked for supplying both reference articles and Figs. 23 and 33. Dr B. Remington, Dr Q. M. Wei and Dr K. Kadau have kindly supplied electronic copies of Figs. 14, 15 and 19 respectively. Professor G. Mayer is thanked for providing helpful comment on behalf of IMR and Professor D. Matlock is thanked for providing IMR key reader assistance with the article, including generous help with formatting of figures and captions. A number of helpful additions to the text have come from reviewers' comments.

References

1. J. Hopkinson: 'On the rupture of iron wire by a blow', *Proc. Manch. Liter. Philos. Soc.*, 1872, **11**, 40–45.
2. J. Hopkinson: 'Further experiments on the rupture of iron wire', *Proc. Manch. Liter. Philos. Soc.*, 1872, **11**, 119–121.
3. J. Hopkinson: 'Original papers', 2–'Scientific papers', 316–324; 1901, Cambridge, Cambridge University Press.
4. B. Hopkinson: 'The effects of momentary stresses in metals', *Proc. R. Soc. Lond.*, 1905, **74**, 498–506.
5. B. Hopkinson: 'A method of measuring the pressure in the detonation of high explosives or by the impact of bullets', *Philos. Trans. R. Soc. Lond. A*, 1914, **213A**, 437–456.
6. J. Niles, S. Nicolich, D. Doll and N. Rasmussen: 'Mitigating the shaped charge jet impact threat in main charge fill ammunition', in 'Advancements in energetic materials and chemical propulsion', (ed. K. K. Kuo and J. de Dios Rivera), 320–330; 2007, New York, Begell House, Inc.
7. A. G. A. Charpy: 'Note sur L'essai des métaux à la flexion par choc de barreaux entaillés', *Mém. CR Soc. Ing. Civ. France*, 1901, 848–877.
8. L. Toth, H.-P. Rossmanith and T. A. Siewert: 'Historical background and development of the Charpy test', in 'From Charpy to present impact testing', (ed. D. Francois and A. Pineau), 3–17; 2002, Amsterdam, Elsevier Science Ltd and European Society for Integrity of Structures.
9. H. Tresca: 'On further applications of the flow of solids', *Proc. Inst. Mech. Eng.*, 1878, **30**, 301–345.
10. W. Johnson: 'Henri Tresca as the originator of adiabatic heat lines', *Int. J. Mech. Sci.*, 1987, **29**, 301–310.
11. W. C. Unwin: 'On the yield point of iron and steel and the effect of repeated straining and annealing', *Proc. R. Soc. Lond.*, 1894, **57**, 178–187.
12. R. W. Armstrong and F. J. Zerilli: 'Dislocation mechanics based viscoplasticity description of fcc, bcc, and hcp metal deformation and fracturing behaviors', in 'Proc. ASME Mater. Div.', MD-69-1, 417–428; 1995, New York, ASME.
13. A. W. McReynolds: 'Plastic waves in aluminum', *Trans. Am. Inst. Min. Metall. Eng.*, 1949, **185**, 32–45.
14. J. A. Ewing: 'On the measurements of small strains in the testing of materials and structures', *Proc. R. Soc. Lond.*, 1895, **58**, 123–142.
15. E. Orowan: 'Notch brittleness and the strength of materials', *Trans. Inst. Eng. Shipb. Scotland*, 1946, **89**, 165–215.
16. J. S. Wark, J. F. Belak, G. W. Collins, J. D. Colvin, H. M. Davies, M. Duchaineau, J. H. Eggert, T. C. Germann, J. Hawreliak, A. Higginbotham, B. L. Holian, K. Kadau, D. H. Kalantar, P. S. Lomdahl, H. E. Lorenzana, M. A. Meyers, B. A. Remington, K. Rosolankova, R. E. Rudd, M. S. Schneider, J. Sheppard and J. S. Stolken: 'Picosecond X-ray diffraction from laser-shocked copper and iron', in 'Shock compression of condensed matter – 2005', (ed. M. D. Furnish *et al.*), CP845, 286–291; 2006, New York, American Institute of Physics.
17. A. Considère: 'Mémoire sur l'emploi du fer et de l'acier dans les constructions', *Ann. Ponts Chauss.*, 1885, **9**, 574–775.
18. N. P. Suh and R. S. Lee: 'A dislocation model for the delayed yielding phenomenon', *Mater. Sci. Eng.*, 1972, **10**, 269–278.
19. W. P. Mason: 'Dislocation drag mechanisms and their effects on dislocation velocities', in 'Dislocation dynamics', (ed. A. R. Rosenfield *et al.*), 487–505; 1968, New York, McGraw-Hill Book Co.
20. A. N. Stroh: 'Force on a moving dislocation', *Phys. Rev.*, 1962, **128**, 55–61.
21. J. P. Hirth and J. Lothe: 'Interaction between moving dislocations', in 'Dislocation dynamics', (ed. A. R. Rosenfield *et al.*), 231–254; 1968, New York, McGraw-Hill Book Co.
22. J. S. Rinehart and J. Pearson: 'Behavior of metals under impulsive loads'; 1954, Metals Park, OH, American Society of Metals.
23. M. A. Meyers: 'Dynamic behavior of materials'; 1994, New York, John Wiley and Sons, Inc.
24. M. Edwards: 'Properties of metals at high rates of strain', *Mater. Sci. Technol.*, 2006, **22**, 453–462.
25. Z. Jeffries: 'Effect of temperature, deformation, and grain size on the mechanical properties of metals', *Trans. Am. Inst. Min. Metall. Eng.*, 1919, **60**, 474–576.
26. F. Osmond and Ch. Frémont: 'Les propriétés mécanique du fer en cristaux isolés', *CR Hebd. Séances Acad. Sci. Paris*, 1905, **141**, 361–363.
27. O. Brezina: 'Untersuchungen uber die zeitgesetze der unelastichen deformation bei zink und flusseisen', *Phys. Z.*, 1923, **24**, 338–344.
28. R. Becker: 'Elastische nachwirkung und plastizität', *Z. Phys.*, 1925, **33**, 185–213.
29. R. Becker: 'Über die plastizität amorpher und kristalliner fester körper', *Phys. Z.*, 1925, **26**, 919–925.
30. R. Becker: 'Plasticity, tenacity and recrystallization (in German)', *Z. Tech. Phys.*, 1926, **7**, 547–555.
31. H. Eyring: 'The activated complex in chemical reactions', *J. Chem. Phys.*, 1935, **3**, 107–115.
32. H. Eyring: 'Viscosity, plasticity, and diffusion as examples of absolute reaction rate theory', *J. Chem. Phys.*, 1936, **4**, 283–291.
33. W. Kauzmann: 'Flow of solid metals from the standpoint of the chemical rate theory', *Trans. Am. Inst. Min. Metall. Eng.*, 1941, **143**, 57–81.
34. F. Seitz and T. A. Read: 'Theory of the plastic properties of solids', *J. Appl. Phys.*, 1941, **12**, 100–118, 170–186, 470–486, 538–554.
35. E. Orowan: 'Zur kristallplastizitat. III: Uber den mechanismus des gleitvorganges', *Z. Phys.*, 1934, **89**, 634–659.
36. M. Polanyi: 'Uber eine art gitterstörung, die einen kristall plastich machen könnte', *Z. Phys.*, 1934, **89**, 660–664.
37. G. I. Taylor: 'The mechanism of plastic deformation of crystals. Part 1. Theoretical', *Proc. R. Soc. Lond. A*, 1934, **145A**, 362ff.
38. E. Schmid and W. Boas: 'Kristallplastizitat'; 1935, Berlin, Julius Springer.
39. E. Orowan: 'Problems of plastic gliding', *Proc. Phys. Soc. Lond.*, 1940, **52**, 8–22.
40. J. M. Burgers and W. G. Burgers: 'Dislocations in crystal lattices', in 'Rheology'; (ed. F. R. Eirich), 141–199; 1956, New York, Academic Press.
41. C. Zener and J. H. Hollomon: 'Effect of strain rate upon plastic flow of steel', *J. Appl. Phys.*, 1944, **15**, 22–32.
42. G. I. Taylor: 'The testing of materials at high rates of mechanical loading', *J. Inst. Civ. Eng.*, 1946, **26**, 486–519.

43. C. S. Barrett and C. T. Haller, Jr: 'Twinning in polycrystalline magnesium', *Trans. Am. Inst. Min. Metall. Eng.*, 1947, **171**, 246–255.
44. G. I. Taylor: 'The use of flat-ended projectiles for determining dynamic yield strength. I. Theoretical considerations', *Proc. R. Soc. Lond. A*, 1948, **194A**, 289–299.
45. A. C. Whiffin: 'The use of flat-ended projectiles for determining yield stress. II. Tests on various metallic materials', *Proc. R. Soc. Lond. A*, 1948, **194A**, 300–322.
46. W. E. Carrington and M. L. V. Gayler: 'The use of flat-ended projectiles for determining yield stress. III. Changes in microstructure caused by deformation at high striking velocities', *Proc. R. Soc. Lond. A*, 1948, **194A**, 323–331.
47. J. B. Hawkyard, D. Eaton and W. Johnson: 'The mean dynamic yield strength of copper and low-carbon steel at elevated temperature from measurements of the mushrooming of flat-ended projectiles', *Int. J. Mech. Sci.*, 1968, **10**, 929–948.
48. D. J. Chapman, D. D. Radford and S. M. Walley: '60 years of Taylor impact and its present use in the study of constitutive relations of materials', Unpublished article.
49. R. M. Davies: 'A critical study of the Hopkinson pressure bar', *Philos. Trans. R. Soc. Lond. A*, 1948, **240A**, 375–457.
50. H. Kolsky: 'An investigation of the mechanical properties of materials at very high rates of strain', *Proc. Phys. Soc. Lond. B*, 1949, **62B**, 676–700.
51. L. R. Oliver, R. W. Armstrong, R. J. Clifton and H. Kolsky: 'Cleavage of zinc crystals induced by stress waves', *Nature*, 1967, **216**, 910.
52. T. von Karman and P. Duwez: 'The propagation of plastic deformation in solids', *J. Appl. Phys.*, 1950, **21**, 987–994.
53. R. W. Armstrong and F. J. Zerilli: 'Dislocation mechanics based analysis of material dynamics behavior', *J. Phys. Fr. Colloq.*, 1988, **49**, (C3), 529–534.
54. J. Harding, E. O. Wood and J. D. Campbell: 'Tensile testing of materials at impact rates of strain', *J. Mech. Eng. Sci.*, 1960, **2**, 88–96.
55. T. Nicholas: 'Tensile testing of materials at high rates of strain', *Exp. Mech.*, 1981, **215**, 177–185.
56. K. A. Hartley, J. Duffy and R. H. Hawley: 'The torsional Kolsky (split Hopkinson) bar', in ''Metals handbook', 9th edn, Vol. 8, 218–228; 1985, Metals Park, OH, American Society for Metals.
57. P. S. Follansbee: 'The Hopkinson bar', in 'Metals handbook', 9th edn, Vol. 8, 198–203; 1985, Metals Park, OH, American Society for Metals.
58. G. T. Gray, III: 'Classic split-Hopkinson pressure bar testing', in 'ASM handbook', Vol. 8, 'Mechanical testing and evaluation', 462–476; 2000, Materials Park, OH, ASM International.
59. J. Klepaczko: 'Application of the split Hopkinson pressure bar to fracture dynamics', *Inst. Phys. Conf. Ser.*, 1980, **47**, 201–214.
60. J. E. Field, W. G. Proud, S. M. Walley and H. T. Goldrein: 'Review of experimental techniques for high rate deformation and shock studies', in 'New experimental methods in material dynamics and impact', (ed. W. K. Nowacki and J. R. Klepaczko), 109–177; 2001, Warsaw, Institute of Fundamental Technological Research.
61. B. W. Dunn: 'A photographic impact testing machine for measuring the varying intensity of an impulsive force', *J. Franklin Inst.*, 1897, **144**, 321–348.
62. K. S. Vecchio and F. Jiang: 'Improved pulse shaping to achieve constant strain rate and stress equilibrium in split Hopkinson pressure bar testing', *Metall. Mater. Trans. A*, 2007, **38A**, 2655–2665.
63. F. Jiang and K. S. Vecchio: 'Dynamic effects in Hopkinson bar four-point bend fracture', *Metall. Mater. Trans. A*, 2007, **38A**, 2896–2906.
64. D. A. Gorham, P. H. Pope and J. E. Field: 'Measurement of stress-strain properties of strong metals at very high strain rates', *Inst. Phys. Conf. Ser*., 1980, **47**, 16–24.
65. D. A. Gorham, P. H. Pope and J. E. Field: 'An improved method for compressive stress-strain measurements at very high strain rates', *Proc. R. Soc. Lond. A*, 1992, **438A**, 153–170.
66. N. A. Safford: 'Materials testing up to $10^5\ s^{-1}$ using a miniaturized Hopkinson bar with dispersion corrections', Proc. 2nd Int. Symp. on 'Intense dynamic loading and its effects', (ed. G. Zhang and S. Huang), 378–383; 1992, Chengdu, Sichuan University Press.
67. D. Jia and K. T. Ramesh: 'A rigorous assessment of the benefits of miniaturization in the Kolsky bar system', *Exp. Mech.*, 2004, **44**, 445–454.
68. C. R. Siviour and J. L. Jordan: 'A miniaturized split Hopkinson pressure bar for very high strain rate testing', Technical Report AFRL-MN-EG-TR-2005-7014, US Air Force Research Laboratory, Eglin, FL, USA, 2005.
69. J. L. Jordan, C. R. Siviour, J. R. Foley and E. N. Brown: 'Compressive properties of extruded PTFE', *Polymer*, 2007, **48**, 4184–4195.
70. A. Seeger: 'Kristallplastizität', in 'Handbuch der physik VII/2, Crystal Physics II', (ed. S. Flugge), 1–210; 1958, Berlin, Springer.
71. A. R. Rosenfield, G. T. Hahn, A. L. Bement, Jr and R. I. Jaffee (eds.): 'Dislocation dynamics'; 1968, New York, McGraw-Hill Book Co.
72. F. J. Zerilli and R. W. Armstrong: 'Dislocation mechanics based constitutive relations for material dynamics calculations', *J. Appl. Phys.*, 1987, **61**, 1816–1825.
73. F. J. Zerilli and R. W. Armstrong: 'Dislocation-mechanics-based constitutive relations for material dynamics modeling: slip and deformation twinning in iron', in 'Shock waves in condensed matter', (ed. S. C. Schmidt and N. C. Holmes), 273–277; 1988, New York, Elsevier Sci. Publ. B.V.
74. F. J. Zerilli and R. W. Armstrong: 'Dislocation mechanics based constitutive relations for dynamic straining to tensile instability', in 'Shock compression of condensed matter – 1989', (ed. S. C. Schmidt *et al.*), 357–361; 1990, New York, Elsevier Sci. Publ. B.V.
75. F. J. Zerilli and R. W. Armstrong: 'Description of tantalum deformation behavior by dislocation mechanics based constitutive relations', *J. Appl. Phys.*, 1990, **68**, 1580–1591.
76. F. J. Zerilli and R. W. Armstrong: 'Modeling shock waves with dislocation mechanics based relations', in 'Shock compression of condensed matter – 1991', (ed. S. C. Schmidt *et al.*), 257–261; 1992, New York, Elsevier Sci. Publ. B.V.
77. F. J. Zerilli and R. W. Armstrong: 'Constitutive relations for titanium and Ti-6Al-4V', in 'Shock compression of condensed matter – 1995', (ed. S. C. Schmidt and W. C. Tao), 315–318; 1996, New York, American Institute of Physics.
78. F. J. Zerilli and R. W. Armstrong: 'Dislocation mechanics based analysis of material dynamics behavior: enhanced ductility, deformation twinning, shock deformation, shear instability, dynamic recovery', *J. Phys. IV France Colloq.*, 1997, **7**, (C3), 637–642.
79. R. W. Armstrong: 'Thermal activation–strain rate analysis (TASRA) for polycrystalline materials', *J. Sci. Ind. Res. (Indian)*, 1973, **32**, 591–598.
80. F. J. Zerilli: 'Dislocation mechanics based constitutive relations', *Metall. Mater. Trans. A*, 2004, **35A**, 2547–2555.
81. R. W. Armstrong: 'Yield and flow stress dependence on polycrystal grain size', in 'Yield, flow and fracture of polycrystals', (ed. T. N. Baker), 1–31; 1983, Barking, Applied Science Publishers.
82. J. Klepaczko: 'Thermally activated flow and strain rate history effects for some polycrystalline fcc metals', *Mater. Sci. Eng.*, 1975, **18**, 121–135.
83. D. E. Eakins and N. N. Thadhani: 'Instrumented Taylor anvil-on-rod impact tests for validating applicability of standard strength models to transient deformation states', *J. Appl. Phys.*, 2006, **100**, 073503-1–073503-8.
84. D. Eakins and N. N. Thadhani: 'Analysis of dynamic mechanical behavior in reverse Taylor anvil-on-rod impact tests', *Int. J. Impact Eng.*, 2007, **34**, 1821–1834.
85. K. G. Hoge and A. K. Mukherjee: 'The temperature and strain rate dependence of the flow stress of tantalum', *J. Mater. Sci.*, 1977, **12**, 1666–1672.
86. S. R. Chen, G. T. Gray, III and S. R. Bingert: in 'Tantalum', (ed. E. Chen *et al.*), 173–184; 1996, Warrendale, PA, TMS.
87. F. J. Zerilli and R. W. Armstrong: 'Constitutive equation for hcp metals and high strength steels', in 'High strain rate effects on polymer, metal and ceramic matrix composites', (ed. Y. D. S. Rajapakse and J. R. Vinson), AD-Vol. 48, 121–126; 1995, New York, American Society of Mechanical Engineers.
88. R. W. Armstrong: 'Theory for the tensile ductile-brittle behavior of polycrystalline hcp materials, with application to beryllium', *Acta Metall.*, 1968, **16**, 347–355.
89. Y. V. R. K. Prasad, N. M. Madhava and R. W. Armstrong: 'The strengthening of hcp materials due to the presence of grain boundaries', in 'Grain boundaries in engineering materials', 67–75; 1975, Baton Rouge, LA, Claitor's Press.
90. P. Rodriguez, R. W. Armstrong and S. L. Mannan: 'The dependence of activation area on grain size in cadmium', *Trans. Ind. Inst. Met.*, 2003, **56**, 189–196.

91. P. Rodriguez: 'Grain size dependence of the activation parameters for plastic deformation: influence of crystal structure, slip system, and rate-controlling dislocation mechanism', *Metall. Mater. Trans. A*, 2004, **35A**, 2697–2705.
92. T. Zhu, J. Li, A. Samanta, H. G. Kim and S. Suresh: 'Interfacial plasticity governs strain rate sensitivity and ductility in nanostructured metals', *Proc. Natl. Acad. Sci.*, 2007, **104**, 3031–3036.
93. Z. Q. Wang, I. J. Beyerlein and R. LeSar: 'The importance of cross-slip in high-rate deformation', *Model. Simul. Mater. Sci. Eng.*, 2007, **15**, 675–690.
94. Z. Q. Wang, I. J. Beyerlein and R. LeSar: 'Dislocation motion in high strain-rate deformation', *Philos. Mag.*, 2007, **87**, 2263–2279.
95. R. W. Armstrong and P. Rodriguez: 'Flow stress/strain rate/grain size coupling for fcc nanopolycrystals', *Philos. Mag.*, 2006, **86**, 5787–5796.
96. R. J. Asaro and S. Suresh: 'Mechanistic models for the activation volume and rate sensitivity in metals with nanocrystalline grains and nano-scale twins', *Acta Mater.*, 2005, **53**, 3369–3382.
97. M. A. Meyers, A. Mishra and D. J. Benson: 'Mechanical properties of nanocrystalline materials', *Prog. Mater. Sci.*, 2006, **51**, 427–556.
98. H. Conrad: 'Plastic deformation kinetics in nanocrystalline fcc metals based on the pile-up of dislocations', *Nanotechnology*, 2007, **18**, 325701.
99. J. J. Gilman: 'The plastic response of solids', in 'Dislocation dynamics', (ed. A. R. Rosenfield *et al.*), 3–25; 1968, New York, McGraw-Hill Book Co.
100. G. Z. Voyiadjis and F. H. Abed: 'Thermomechanical response of metals with different crystal structures at high strain rates and temperatures', in 'Dislocations, plasticity, damage, and metal forming: material response and multiscale modeling', (ed. A. S. Khan and A. R. Khoei), 382–384; 2005, Fulton, MD, Neat Press.
101. G. Z. Voyiadjis and F. H. Abed: 'Microstructural based models for bcc and fcc metals with temperature and strain rate dependency', *Mech. Mater.*, 2005, **37**, 355–378.
102. F. H. Abed and G. Z. Voyiadjis: 'A consistent modified Zerilli–Armstrong flow stress model for BCC and FCC metals at elevated temperatures', *Acta Mech.*, 2005, **175**, 1–18.
103. G. R. Johnson and W. H. Cook: 'A constitutive model and data for metals subjected to large strains, high strain rates, and high temperatures', Proc. 7th Int. Symp. on 'Ballistics', The Hague, The Netherlands, 1983, American Defense Preparedness Association, 541–547.
104. G. R. Johnson and W. H. Cook: 'Fracture characteristics of three metals subjected to various strains, strain rates, temperatures, pressures', *Eng. Fract. Mech.*, 1985, **21**, 31–48.
105. B. Langrand, P. Geoffroy, J.-L. Petitniot, J. Fabis, E. Markiewicz and P. Drazetic: 'Identification technique of constitutive model parameters for crashworthiness modeling', *Aerospace Sci. Technol.*, 1999, **4**, 215–227.
106. S. Nemat-Nasser, Y.-F. Li and J. B. Isaacs: 'Experimental/computational valuation of flow stress at high strain rates with application to adiabatic shear banding', *Mech. Mater.*, 1994, **17**, 111–134.
107. R. E. Reed, H. D. Guberman and R. W. Armstrong: 'Effect of neutron irradiation on the temperature dependence of the flow stress of niobium single crystals', *Phys. Status Sol.*, 1970, **37**, 647–655.
108. P. S. Follansbee and U. F. Kocks: 'A constitutive description of the deformation of copper based on the use of the mechanical threshold stress as an internal state variable', *Acta Metall.*, 1988, **36**, 81–93.
109. G. T. Gray, III, S. R. Chen and K. S. Vecchio: 'Influence of grain size on the constitutive response and substructure evolution of Monel 400', *Metall. Mater. Trans. A*, 1999, **30A**, 1235–1247.
110. B. Holmedal: 'On the formulation of the mechanical threshold stress model', *Acta Mater.*, 2007, **55**, 2739–2746.
111. D. J. Steinberg, S. G. Cochran and M. W. Guinan: 'A constitutive model for metals applicable at high strain rates', *J. Appl. Phys.*, 1980, **51**, 1498–1504.
112. S. R. Bodner and Y. Partom: 'Constitutive equations for elasto-viscoplastic strain-hardening materials', *J. Appl. Mech.*, 1975, **42**, 385–389.
113. B. A. Remington, P. Allen, E. M. Bringa, J. Hawreliak, D. Ho, K. T. Lorenz, H. Lorenzana, J. M. McNaney, M. A. Meyers, S. W. Pollaine, K. Rosolankova, B. Sadik, M. S. Schneider, D. Swift, J. Wark and B. Yaakobi: 'Material dynamics under extreme conditions of pressure and strain rate', *Mater. Sci. Technol.*, 2006, **22**, 474–488.
114. T. C. Germann, D. Tanguy, B. L. Holian, P. S. Lomdahl, M. Mareschal and R. Ravelo: 'Dislocation structure behind a shock front in fcc perfect crystals: atomistic simulation results', *Metall. Mater. Trans. A*, 2004, **35A**, 2609–2615.
115. K. Kadau, T. C. Germann, P. S. Lomdahl, B. L. Holian, D. Kadau, P. Entel, M. Kreth, F. Westerhoff and D. E. Wolf: 'Molecular-dynamics study of mechanical deformation in nanocrystalline aluminum', *Metall. Mater. Trans. A*, 2004, **35A**, 2719–2723.
116. R. A. Lebensohn, E. M. Bringa and A. Caro: 'A viscoplastic micromechanical model for the yield strength of nanocrystalline materials', *Acta Mater.*, 2007, **55**, 261–271.
117. A. Cao, E. M. Bringa and M. A. Meyers: 'Shock compression of monocrystalline copper: atomistic simulations', *Metall. Mater. Trans. A*, 2007, **38A**, 2681–2688.
118. P. Rodriguez and R. W. Armstrong: 'Strength and strain rate sensitivity for hcp and fcc nanopolycrystal metals', *Bull. Mater. Sci. (Ind.)*, 2006, **29**, 717–720.
119. A. S. Argon and S. Yip: 'The strongest size', *Philos. Mag. Lett.*, 2006, **86**, 713–720.
120. J. M. Krafft, A. M. Sullivan and G. R. Irwin: 'Relationship between the fracture ductility transition and strain hardening characteristics of a low carbon steel', *J. Appl. Phys.*, 1957, **28**, 379–380.
121. A. H. Cottrell: 'Theory of brittle fracture in steel and similar metals', *Trans. TMS-AIME*, 1958, **212**, 192–203.
122. N. J. Petch: 'The ductile-brittle transition in the fracture of alpha-iron', *Philos. Mag.*, 1958, **3**, 1089–1127.
123. J. D. Campbell, R. H. Cooper and T. J. Fischhof: 'The dynamics of non-uniform plastic flow in low-carbon steel', in 'Dislocation dynamics', 723–746; 1968, New York, McGraw-Hill Book Co.
124. A. R. Rosenfield, E. Votava and G. T. Hahn: 'Dislocations and the ductile-brittle transition', in 'Ductility', 63–85; 1968, Metals Park, OH, American Society of Metals.
125. R. W. Armstrong: 'The (cleavage) fracture strength of pre-cracked polycrystals', *Eng. Fract. Mech.*, 1987, **28**, 529–538.
126. R. W. Armstrong, G. R. Irwin and X. J. Zhang: 'Microstructural mechanics description of cleavage fracturing', in 'Cleavage fracture: George R. Irwin Symposium', 51–58; 1998, Warrendale, PA, TMS.
127. R. Sandstrom and Y. Bergstrom: 'Relationship between Charpy V transition temperature in mild steel and various material parameters', *Met. Sci.*, 1984, **18**, 177–186.
128. G. R. Irwin: 'Fracture', in 'Encyclopedia of physics VI', (ed. S. Flugge), 551–590; 1958, Berlin, Springer.
129. G. R. Irwin: 'Fracture mechanics', in 'Metals handbook', Vol. 8, 439–458; 1985, Metals Park, OH, American Society of Metals.
130. J. F. Kalthoff: 'On the measurement of dynamic fracture toughness – a review of recent work', *Int. J. Fract.*, 1985, **27**, 277–298.
131. G. S. Pisarenko, A. Y. Krasowsky, V. A. Vainshtock, I. V. Kramerenko and V. N. Krasiko: 'The combined micro- and macro-fracture mechanics approach to engineering problems of strength', *Eng. Fract. Mech.*, 1987, **28**, 539–554.
132. M. S. Wechsler: 'Radiation embrittlement in the pressure-vessel steels of nuclear power plants', *J. Met.*, 1989, **41**, (12), 7–14.
133. J. D. Landes: 'Fracture mechanics and the nuclear industry', *Metall. Trans. A*, 1990, **21A**, 1097–1104.
134. N. J. Petch and R. W. Armstrong: 'Work hardening in cleavage fracture toughness', *Acta Metall. Mater.*, 1989, **37**, 2279–2285.
135. H. C. Rogers: 'Adiabatic shearing: a review', *Ann. Rev. Mater. Sci.*, 1979, **9**, 283–311.
136. S. P. Timothy: 'The structure of adiabatic shear bands in metals: a critical review', *Acta Metall.*, 1987, **35**, 301–306.
137. S. M. Walley: 'Shear localization: a historical overview', *Metall. Mater. Trans. A*, 2007, **38A**, 2629–2654.
138. Y. Bai and B. Dodd: 'Adiabatic shear localization: occurrence, theories and applications', 1992; Oxford, Pergamon Press.
139. R. W. Armstrong, R. C. Batra, M. A. Meyers and T. W. Wright (eds.): 'Shear instabilities and viscoplasticity theories', *Mech. Mater.*, 1994, **17**, 83–328.
140. Q. Wei: 'Strain rate effects in the ultrafine grain and nanocrystalline regimes – influence on some constitutive responses', *J. Mater. Sci.*, 2007, **42**, 1709–1727.
141. R. W. Armstrong and F. J. Zerilli: 'Dislocation mechanics aspects of plastic instability and shear banding', *Mech. Mater.*, 1994, **17**, 319–327.
142. N. J. Petch and R. W. Armstrong: 'The tensile test', *Acta Metall. Mater.*, 1990, **38**, 2695–2700.

143. G. Z. Voyiadjis and F. H. Abed: 'A coupled temperature and strain rate dependent yield function for dynamic deformation of bcc metals', *Int. J. Plast.*, 2006, **22**, 1398–1431.
144. G. Z. Voyiadjis and F. H. Abed: 'Transient localizations in metals using microstructure-based yield surfaces', *Model. Simul. Mater. Sci. Eng.*, 2007, **15**, 583–595.
145. L. P. Kubin, Ph. Spiesser and Y. Estrin: 'Computer simulation of the low temperature instability of plastic flow', *Acta Metall.*, 1982, **30**, 385–394.
146. A. Marchand and J. Duffy: 'An experimental study of the formation process of adiabatic shear bands in a structural steel', *J. Mech. Phys. Sol.*, 1988, **36**, 251–283.
147. M. A. Meyers, Y.-J. Chen, F. D. S. Marquis and D. S. Kim: 'High strain, high-strain-rate behavior of tantalum', *Metall. Mater. Trans. A*, 1995, **26A**, 2493–2501.
148. Y.-J. Chen, M. A. Meyers and V. F. Nesterenko: 'Spontaneous and forced shear localization in high-strain-rate deformation of tantalum', *Mater. Sci. Eng. A*, 1999, **A268**, 70–82.
149. T. W. Wright: 'The physics and mathematics of adiabatic shear bands'; 2002, Cambridge, Cambridge University Press.
150. V. F. Nesterenko: 'Dynamics of heterogeneous materials'; 2001, New York, Springer-Verlag.
151. R. C. Batra and L. Chen: 'Effect of viscoplastic relations on the instability strain, shear band initiation strain, and the strain corresponding to the minimum shear band spacing, and the band width in a thermo-viscoplastic material', *Int. J. Plast.*, 2001, **17**, 1465–1489.
152. T. Rabczuk, P. M. A. Areias and T. Belytschko: 'A simplified mesh-free method for shear bands with cohesive surfaces', *Int. J. Numer. Meth. Eng.*, 2007, **69**, 993–1021.
153. F. J. Zerilli and R. W. Armstrong: 'Dislocation mechanics based constitutive equation incorporating dynamic recovery and applied to thermomechanical shear instability', in 'Shock compression of condensed matter – 1997', (ed. S. C. Schmidt *et al.*), CP 429, 215–218; 1998, Melville, NY, American Institute of Physics.
154. R. W. Armstrong, C. S. Coffey and W. L. Elban: 'Adiabatic heating at a dislocation pile-up avalanche', *Acta Metall.*, 1982, **30**, 2111–2118.
155. R. W. Armstrong and W. L. Elban: 'Temperature rise at a dislocation pile-up breakthrough', *Mater. Sci. Eng. A*, 1989, **A122**, L1–L3.
156. R. W. Armstrong and W. R. Grise: 'Hot spots from dislocation pile-up avalanches', in 'Shock compression of condensed matter – 2005', (ed. M. D. Furnish *et al.*), CP 845, 1033–1036; 2006, Melville, NY, American Institute of Physics.
157. M. A. Meyers, G. Subhash, B. K. Kad and L. Prasad: 'Evolution of microstructure and shear-band formation in α-titanium', *Mech. Mater.*, 1994, **17**, 175–193.
158. K.-H. Hartmann, H.-D. Kunze and L. W. Meyer: 'Metallurgical effects on impact loaded materials', in 'Shock-wave and high-strain-rate phenomena in metals', (ed. M. A. Meyers and L. E. Murr), 325–337; 1981, New York, Marcel Dekker.
159. W. H. Holt, W. Mock, Jr, W. G. Soper, C. S. Coffey, V. Ramachandran and R. W. Armstrong: 'Reverse-ballistic impact study of shear plug formation and displacement in Ti6Al4V alloy', *J. Appl. Phys.*, 1993, **73**, 3753–3759.
160. F. Martinez, L. E. Murr, A. Ramirez, S. M. Lopez and S. M. Gaytan: 'Dynamic deformation and adiabatic shear microstructures associated with ballistic plug formation and fracture in Ti6Al4V targets', *Mater. Sci. Eng. A*, 2007, **A454**–**A455**, 581–589.
161. L. S. Magness, Jr: 'High strain rate deformation behaviors of kinetic energy penetrator materials during ballistic impact', *Mech. Mater.*, 1994, **17**, 147–154.
162. L. Zernow and E. J. Chapyak: 'Direct experimental evidence of melting on a shear band in a molybdenum shaped charge slug', in 'Metallurgical and materials applications of shock-wave and high-strain-rate phenomena', (ed. L. E. Murr *et al.*), 479–486; 1995, Amsterdam, Elsevier Science B.V.
163. S. Pappu and L. E. Murr: 'Hydrocode and microstructural analysis of explosively formed penetrators', *J. Mater. Sci.*, 2002, **37**, 233–248.
164. C. Kennedy and L. E. Murr: 'Comparison of tungsten heavy-alloy rod penetration into ductile and hard metal targets: microstructural analysis and computer simulations', *Mater. Sci. Eng. A*, 2002, **A325**, 131–143.
165. O. L. Valerio-Flores, L. E. Murr, V. Hernandez and S. Quinones: 'Observations and simulations of the low velocity-to-hypervelocity impact crater transition for a range of penetrator densities into thick aluminum targets', *J. Mater. Sci.*, 2004, **39**, 6271–6289.
166. C. Pizana, L. E. Murr, M. T. Baquera, I. A. Anchondo, A. Putrevu, C. Y. Pina, T. C. Tamoria, H. C. Chen and S. J. Cytron: 'Solid-state flow, mechanical alloying, and melt-related phenomena for [001] single-crystal W ballistic rod penetrators interacting with steel targets', *Mater. Sci. Eng. A*, 2006, **A428**, 301–313.
167. S. Dey, T. Borvik, O. S. Hopperstad and M. Langseth: 'On the influence of constitutive relation in projectile impact in steel plates', *Int. J. Impact Eng.*, 2007, **34**, 464–486.
168. R. G. McQueen, S. P. Marsh, J. W. Taylor and W. J. Carter: 'The equation of state of solids from shock-wave studies', in 'High velocity impact phenomena', (ed. R. Kinslow), Chapter 6, 293–417, 515–568; 1970, New York, Academic Press.
169. C. S. Smith: 'Metallographic studies of metals after explosive shock', *Trans. TMS-AIME*, 1958, **212**, 574–589.
170. J. Weertman and P. S. Follansbee: 'Dislocation dynamics and plastic shock waves', *Mech. Mater.*, 1988, **7**, 177–189.
171. G. T. Gray, III: 'Shock wave testing of ductile materials', in 'ASM materials handbook', Vol. 8, 'Mechanical testing', 530–538; 2000, Materials Park, OH, ASM International.
172. E. M. Bringa, K. Rosolankova, R. E. Rudd, B. A. Remington, J. S. Wark, M. Duchaineau, D. H. Kalantar, J. Hawreliak and J. Belak: 'Shock deformation of face-centered-cubic metals on subnanosecond timescales', *Nat. Mater.*, 2006, **5**, 805–809.
173. R. J. Jensen, P. A. Rigg, M. D. Knudsen, R. S. Hixson, G. T. Gray, III, B. H. Sensor and F. J. Cherna: 'Dynamic compression of iron single crystals', in 'Shock compression of condensed matter – 2005', (ed. M. D. Furnish *et al.*), CP845, Part 1, 232–235; 2006, Melville, NY, American Institute of Physics.
174. P. S. Follansbee, G. Regazzoni and U. F. Kocks: 'The transition in drag-controlled deformation in copper at high strain rates', *Inst. Phys. Conf. Ser.* 1984, **70**, 71–80.
175. R. W. Armstrong, V. Ramachandran and F. J. Zerilli: 'Dislocation mechanics description of dynamic plasticity and fracturing properties', in 'Advances in materials and applications', (ed. P. R. Rao), 201–229; 1994, New Delhi, Wiley Eastern, Ltd.
176. F. J. Zerilli and R. W. Armstrong: 'The effect of dislocation drag on the stress-strain behavior of fcc metals', *Acta Mater.*, 1992, **40**, 1803–1808.
177. G. T. Gray III, E. Cerreta, C. A. Yablinsky, L. B. Addessio, B. L. Henrie, B. H. Sencer, M. Burkett, P. J. Maudlin, S. A. Maloy, C. P. Trujillo and M. F. Lopez: 'Influence of shock pre-straining and grain size on the dynamic-tensile-extrusion response of copper: experiments and simulation', in 'Shock compression of condensed matter – 2005', (ed. M. D. Furnish *et al.*), CP845, Part 2, 7725–7728; 2006, Melville, NY, American Institute of Physics.
178. R. W. Armstrong: 'Strength and ductility of metals', *Trans. Ind. Inst. Met.*, 1997, **50**, 521–531.
179. M. A. Meyers: 'A mechanism for dislocation generation in shock-wave deformation', *Scr. Metall.*, 1978, **12**, 21–26.
180. M. A. Shehadeh, H. M. Zbib and T. D. de la Rubia: 'Modelling the dynamic deformation and patterning in fcc single crystals at high strain rates: dislocation dynamics plasticity analysis', *Philos. Mag.*, 2005, **85**, 1667–1685.
181. M. A. Shehadeh, H. M. Zbib and T. Diaz de la Rubia: 'Multiscale dislocation dynamics simulations of shock compression in copper single crystal', *Int. J. Plast.*, 2005, **21**, 2369–2390.
182. M. A. Shehadeh, E. M. Bringa, H. M. Zbib, J. M. McNaney and B. A. Remington: 'Simulation of shock-induced plasticity including homogeneous and heterogeneous dislocation nucleations', *Appl. Phys. Lett.*, 2006, **89**, 171918.
183. R. W. Armstrong (transl. J. Boileau): 'Roles possibles des dislocations dans les detonations par choc dans les cristeaux energetique', *Rev. Scient. Tech. Defence*, 1992, **16**, (2), 162–165.
184. F. A. Bandak, R. W. Armstrong, A. S. Douglas and D. H. Tsai: 'Dislocation structures for shock strengthening', in 'Shock compression of condensed matter – 1991', (ed. S. C. Schmidt *et al.*), 559–561; 1992, New York, Elsevier Sci. Publ. B.V.
185. F. A. Bandak, R. W. Armstrong and A. S. Douglas: 'Dislocation structure for one-dimensional strain in a shocked crystal', *Phys. Rev. B*, 1992, **46B**, 3228–3235.
186. F. A. Bandak, D. H. Tsai, R. W. Armstrong and A. S. Douglas: 'Formation of nanodislocation dipoles in shock-compressed crystals', *Phys. Rev. B*, 1993, **47B**, 11681–11687.
187. R. W. Armstrong, W. Arnold and F. J. Zerilli: 'Dislocation mechanics of shock induced plasticity', *Metall. Mater. Trans. A*, 2007, **38A**, 2605–2610.
188. J. W. Swegle and D. E. Grady: 'Shock viscosity and the prediction of shock wave rise times', *J. Appl. Phys.*, 1985, **58**, 692–701.

189. T. Zhu, J. Li, A. Samanta, A. Leach and K. Gall: 'Temperature and strain-rate dependence of surface dislocation nucleation', *Phys. Rev. B*, Unpublished article.
190. M. A. Tschopp and D. L. McDowell: 'Influence of single crystal orientation on homogeneous dislocation nucleation under uniaxial loading', *J. Mech. Phys. Sol.*, to be published.
191. W. Arnold: 'Dynamisches Werkstoffverhalten von Armco-Eisen Stosswellbelastung', Fortschrittberichte VDI, 5, 247; 1992, Dusseldorf, VDI-Verlag GmbH.
192. L. E. Murr, M. A. Meyers, C.-S. Niou, Y.-J. Chen, S. A. Pappu and C. Kennedy: 'Shock induced deformation twinning in tantalum', *Acta Mater.*, 1997, **45**, 157–175.
193. M. A. Meyers: 'Dynamic deformation and failure', in 'Mechanics and materials: fundamentals and linkages', (ed. M. A. Meyers *et al.*), Chapter 14, 489–594; 1999, New York, John Wiley and Sons, Inc.
194. B. Y. Cao, M. A. Meyers, D. H. Lassila, M. S. Schneider, Y. B. Xu, D. H. Kalantar and B. A. Remington: 'Defect substructures in plate impacted and laser shocked monocrystalline copper', in 'Shock compression of condensed matter – 2005', (ed. M. D. Furnish *et al.*), CP845, Part 2, 1145–1148; 2006, Melville, NY, American Institute of Physics.
195. B. Y. Cao, M. A. Meyers, D. H. Lassila, M. S. Schneider, Y. B. Xu, D. H. Kalantar and B. A. Remington: 'Effect of shock compression method on the defect structure in single crystal copper', *Mater. Sci. Eng. A*, 2005, **A409**, 270–281.
196. H. Jarmakani, J. M. McNaney, M. S. Schneider, D. Orlikowski, J. H. Nguyen, B. Kad and M. A. Meyers: 'Dynamic response of [single crystalline] copper subjected to quasi-isentropic gas-gun driven loading', in 'Shock compression of condensed matter – 2005', (ed. M. D. Furnish *et al.*), CP845, Part 2, 1319–1322; 2006, Melville, NY, American Institute of Physics.
197. H. Jarmakani, J. M. McNaney, M. S. Schneider, D. Orlikowski, J. H. Nguyen, B. Kad and M. A. Meyers: 'Dynamic response of single crystalline copper subjected to quasi-isentropic, gas-gun loading', *Mater. Sci. Eng. A*, 2007, **A463**, 249–262.
198. R. W. Armstrong, W. Arnold and F. J. Zerilli: 'Dislocation mechanics under extreme pressures', in 'Shock compression of condensed matter – 2007', (ed. M. L. Elert *et al.*), CP955, Part 1, 623–626; 2007, Melville, NY, American Institute of Physics.
199. L. E. Murr and E. V. Esquivel: 'Observations of common microstructural issues associated with dynamic deformation phenomena: twins, microbands, grain size effects, shear bands, and dynamic recrystallization', *J. Mater. Sci.*, 2004, **39**, 1153–1168.
200. R. W. Armstrong and F. J. Zerilli: 'Deformation twinning: from atomic modeling to shock wave loading', in 'Advances in twinning', (ed. S. Ankem and C. S. Pande), 67–81; 1999, Warrendale, PA, TMS.
201. R. W. Armstrong and F. J. Zerilli: 'Dislocation mechanics aspects of shock-wave and high-strain-rate phenomena', in 'Fundamental issues and applications of shock-wave and high-strain-rate phenomena', (ed. K. P. Staudhammer *et al.*), Chapter 15, 115–124; 2001, Oxford, Elsevier Sci. Publ.
202. V. F. Moiseev and V. I. Trefilov: 'Change of the deformation mechanism (slip vs twinning) in polycrystalline alpha-iron', *Phys. Status Sol.*, 1966, **18**, 881–895.
203. N. M. Madhava, P. J. Worthington and R. W. Armstrong: 'Discontinuous twinning during essentially elastic compression of steel', *Philos. Mag.*, 1972, **25**, 519–522.
204. J. B. McKirgan: 'Microstructurally-based EPIC simulations of Taylor impact tests', MSc thesis, University of Maryland, College Park, MD, USA, 1990.
205. G. T. Gray, III: 'Deformation twinning in Al-4·8 wt% Mg', *Acta Metall.*, 1988, **36**, 1745–1754.
206. L. E. Murr, E. A.Trillo, S. Pappu and C. Kennedy: 'Adiabatic shear bands and examples of their role in severe plastic deformation', *J. Mater. Sci.*, 2002, **37**, 3337–3360.
207. J. F. C. Lins, H. R. Z. Sandim, H.-J. Kestenbach, D. Raabe and K. S. Vecchio: 'A microstructural investigation of adiabatic shear bands in an interstitial free steel', *Mater. Sci. Eng. A*, 2007, **A457**, 205–218.
208. Q. Xue, E. K. Cerreta and G. T. Gray, III: 'Microstructural characteristics of post-shear localization in cold-rolled 316L stainless steel', *Acta Mater.*, 2007, **55**, 691–704.
209. B. Y. Yang, M. A. Meyers, D. H. Lassila, M. S. Schneider, Y. B. Xu, D. H. Kalantar and B. A. Remington: 'Defect substructures in plate impacted and laser shocked monocrystalline copper', in 'Shock compression of condensed matter – 2005', (ed. M. D. Furnish *et al.*), CP 845, 1145–1148; 2006, Melville, NY, American Institute of Physics.
210. E. V. Esquivel and L. E. Murr: 'Deformation effects in shocked metals and alloys', *Mater. Sci. Technol.*, 2006, **22**, 438–452.
211. L. E. Murr and C. Pizana: 'Dynamic recrystallization: the dynamic deformation regime', *Metall. Mater. Trans. A*, 2007, **38A**, 2611–2628.
212. S. N. Medyanik, W. K. Liu and S. Li: 'On criteria for dynamic adiabatic shear band propagation', *J. Mech. Phys. Sol.*, 2007, **55**, 1439–1461.
213. S. A. Quinones and L. E. Murr: 'Correlations of computed simulations with residual hardness mapping and microstructural observations of high velocity and hypervelocity impact craters in copper', *Phys. Status Sol. (a)*, 1998, **166**, 763–789.
214. J. M. Wells and R. M. Brannon: 'Advances in X-ray computed tomography diagnostics of ballistic impact damage', *Metall. Mater. Trans. A*, 2007, **38A**, 2943–2949.
215. L. Seaman: 'Fracture and fragmentation under shock loading', in 'Shock and vibration computer programs', (ed. W. Pilkey and B. Pilkey), 563–577; 1975, Charlottesville, VA, University of Virginia.
216. L. Seaman, D. R. Curran and D. A. Shockey: 'Computational models for ductile and brittle fracture', *J. Appl. Phys.*, 1976, **47**, 4814–4826.
217. V. I. Romanchenko and G. V. Stepanov: 'Dependence of the critical stress on the loading time parameters during spall in copper, aluminum and steel', *J. Appl. Mech. Tech. Phys. (Russ.)*, 1980, **21**, 555–561.
218. V. Panov, R. Vignjevic, N. Bourne and J. Millet: 'Material modeling at high strain rate', in 'Shock compression of condensed matter – 2005', (ed. M. D. Furnish *et al.*), CP845, Part 1, 646–649; 2006, New York, American Institute of Physics.
219. D. E. Grady: 'The statistical fragmentation theory of N.F. Mott', in 'Shock compression of condensed matter – 2003', (ed. M. D. Furnish *et al.*), CP 706, Part 1, 455–458; 2004, Melville, NY, American Institute of Physics.
220. R. M. Brannon, J. M. Wells and O. E. Strack: 'Validating theories for brittle damage', *Metall. Mater.Trans. A*, 2007, **38A**, 2861–2868.
221. M. D. Furnish, W. M. Trott, J. Mason, J. Podsednik, W. D. Reinhart and C. Hall: 'Assessing mesoscale material response via high-resolution line-imaging VISAR', in 'Shock compression of condensed matter – 2003', (ed. M. D. Furnish *et al.*), CP706, Part 2, 1159–1162; 2004, Melville, NY, American Institute of Physics.
222. M. D. Furnish, W. D. Reinhart, W. M. Trott, L. C. Chhabildas and T. J. Vogler: 'Variability in dynamic properties of tantalum: spall, Hugoniot elastic limit and attenuation', in 'Shock compression of condensed matter – 2005', (ed. M. D. Furnish *et al.*), CP 845, 615–618; 2006, Melville, NY, American Institute of Physics.
223. S. R. Greenfield, J. L. Casson and A. C. Koskelo: 'Nanosecond interferometric studies of surface deformation induced by laser irradiation', *Proc. SPIE – Int. Soc. Opt. Eng.*, 2000, **3902**, 108–117.
224. A. C. Koskelo, S. R. Greenfield, D. Greening and D. Swift: 'New windows into shocks at the mesoscale', in 'Shock compression of condensed matter – 2003', (ed. M. D. Furnish *et al.*), CP706, Part 1, 239–242; 2004, Melville, NY, American Institute of Physics.
225. A. C. Koskelo, S. R. Greenfield, K. McClellan, D. Byler, R. Dickerson, D. Paisley, S. Luo, D. Swift, D. Tonks and P. Peralta: 'Dynamics of the onset of damage in metals under shock loading', in 'Shock compression of condensed matter – 2007', (ed. M. L. Elert *et al.*), CP955, Part 1, 557–560; 2007, Melville, NY, American Institute of Physics.